water

MDPI

Article

Reconstruction of Paleoenvironment and Paleoclimate of the Neogene Guantao Formation in the Liaodong Sub-Uplift of Bohai Bay Basin in China by Sedimentary Geochemistry Methods

Maolin Wang [1,2,†], Yuanhua Qing [3,*,†], Zheyuan Liao [4], Yuefeng Li [4], Sheng Li [5], Zhengxiang Lv [4,6,†], Shijun Ni [1], Jin Fang [2], Song Tang [2] and Yawen Yang [7]

1 College of Earth Science, Chengdu University of Technology, Chengdu 610059, China
2 Central Sichuan Oil and Gas District, PetroChina Southwest Oil & Gasfield Company, Suining 629000, China
3 School of History and Geography, Chengdu Normal University, Chengdu 611130, China
4 College of Energy Resources, Chengdu University of Technology, Chengdu 610059, China
5 Yunnan Earthquake Agency, Kunming 650224, China
6 State Key Laboratory of Oil–Gas Reservoirs Geology and Exploitation, Chengdu University of Technology, Chengdu 610059, China
7 Natural Gas Economy Research Institute, PetroChina Southwest Oil & Gasfield Company, Chengdu 610051, China
* Correspondence: 051061@cdnu.edu.cn
† These authors contributed equally to this work.

Citation: Wang, M.; Qing, Y.; Liao, Z.; Li, Y.; Li, S.; Lv, Z.; Ni, S.; Fang, J.; Tang, S.; Yang, Y. Reconstruction of Paleoenvironment and Paleoclimate of the Neogene Guantao Formation in the Liaodong Sub-Uplift of Bohai Bay Basin in China by Sedimentary Geochemistry Methods. *Water* **2022**, *14*, 3915. https://doi.org/10.3390/w14233915

Academic Editors: Joaquim Pais-Barbosa and Diogo Mendes

Received: 1 September 2022
Accepted: 21 November 2022
Published: 1 December 2022

Abstract: The paleosedimentary environment and paleoclimate of the Neogene Guantao Formation in the Liaodong sub-uplift of Bohai Bay Basin in China, which is an important oil and gas exploration horizon, are not clear owing to the lack of quantitative analysis. The paleosedimentary environment and paleoclimate can be qualitatively or semi-quantitatively reconstructed by sedimentary geochemical indicators sensitive to the environment and climate. Based on the evaluation of whether the elements and isotopes can effectively record paleosedimentary environment and paleoclimate information or not, the paleoclimate (temperature and humidity), paleoenvironment (salinity, water depth, redox conditions), and evolution of the paleoenvironment and paleoclimate are studied by analyzing the trace elements, carbon and oxygen isotopes, strontium isotopes, whole-rock mineral compositions, and clay minerals of mudstones of the Guantao Formation in the Liaodong sub-uplift, Bohai Bay Basin. The study results show that (1) according to the trace element distribution patterns, high concentrations of continental elements (Ti, Zr, Th), clay minerals, and detrital content, the Guantao Formation is a product of proximal deposits, and the provenance mainly originates from the intermediate–acidic magmatic rocks near surrounding uplifts. (2) The paleoclimate during the sedimentation of the Guantao Formation was mainly semi-arid and semi-humid, as revealed by the Sr/Cu ratio. However, the high Rb/Sr and $^{87}Sr/^{86}Sr$ ratios demonstrate that the paleoclimate is relatively warm and humid. (3) The paleosedimentary temperature calculated by the Sr content and $\delta^{18}O$ is roughly 30 °C, indicating that the Guantao Formation was deposited in a subtropical to tropical climate. (4) The Guantao Formation was deposited in continental freshwater according to the Li, Ni, and Sr content, Sr/Ba ratios, $^{87}Sr/^{86}Sr$ ratios, and salinity index Z. (5) The water depth of the paleoenvironment of the Guantao Formation is mainly in nearshore shallow water, reflected by the Mn/Ti ratio and calculated by the Co content, and the oxidizing condition of the paleoenvironment of the Guantao Formation, reflected by the U/Th, V/Cr, and Ni/Co ratios, is in a good coupling relationship with this environment. (6) As revealed by the variations in the geochemical data in the section, the temperature, humidity, and water depth of the Guantao Formation gradually increased from the early to late period, while the salinity gradually decreased, and the chemical weathering effect gradually increased.

Keywords: trace element; isotope; paleowater depth; paleosalinity; paleosedimentary temperature; redox state

1. Introduction

The sedimentary environment is defined by physical (such as current activity, water depth, climate, tectonism, and volcanism), chemical (such as solution, precipitation), and biological parameters [1,2]. The sedimentary environment has an important influence on hydrocarbon accumulation by controlling the distribution of source and reservoir rocks [3,4]. Thus, to a great extent, the reconstruction of the paleoenvironment can help geologists to explore oil and gas enrichment zones. Sedimentary geochemistry is concerned with the chemical investigation of the geological processes and materials of sedimentary systems [5]. Compared with traditional sedimentological research methods based on macroscopic descriptive characteristics such as the color of rock, lithology, sedimentary structure, and fossils, sedimentary geochemistry, as a quantitative method, uses the geological process information of elements and isotopes that are difficult to identify with the naked eye to precisely reveal the mysteries of sedimentary phenomena [6,7]. In recent 30 years, the development of X-ray spectrometry, electron probes, energy spectra, micro-area sampling, and other high-precision analysis technologies has greatly promoted the progress of sedimentary geochemistry theory and methods [8,9]. The major elements, trace elements, rare earth elements, and isotopic geochemistry methods have been widely used in the paleoclimate and diagenesis research fields, and a variety of discriminant indexes and empirical formulas have been established, which has caused sedimentary geochemistry to develop from qualitative to quantitative. For example, [7–10] established baseline data on geochemical elemental concentrations in estuarine sediments and their seasonal variations in the surface sediments of the Manakudi estuary, Southwest India.

Sedimentary geochemical parameters are influenced by tectonism, source materials, the opening degree of the sedimentary environment, diagenesis, biology, and so on [11–14]. Therefore, when applying sedimentary geochemistry to judge the sedimentary environment, it is necessary to first select the samples that are not subject to diagenetic alterations [15,16], and the terrigenous influence should be eliminated using some specific methods [13,14]; moreover, it is necessary to adopt geochemical indexes that are sensitive to the sedimentary environment and are relatively stable in the latter diagenetic process [17–19]. It has been proven that fine-grained rocks such as mudstones are effective carriers of primary sedimentary geochemical information [17,20]. The detrital flux could be checked by the reliability coefficient or the crossplot between a given trace element and a terrigenous element, such as Al, Zr, or Ti, and the authigenic fraction of elements could be estimated as the excess of the average mudstone abundance [14,21]. Tribovillard et al. (2006) stated that the combined use of U, V, and Mo enrichment may allow one to distinguish suboxic environments from anoxic–euxinic ones according to the synthesis of the geochemical behavior of certain trace elements and previous paleoenvironmental reconstruction works [14].

Environmental sensitivity differences in elements and isotopes result in chemical behavior differentiation, so different geochemical indicators, including specific element content, ratios, and indexes calculated by several elements, can reflect different sedimentary environment characteristics [7,14,22]. According to environmental sensitivity, geochemical indicators could be roughly classified as follows: (1) environmental type, including provenance (Zr/Hf, $^{87}Sr/^{86}Sr$), redox (DOP, V/Ni, U/Th, authigenic U, V/Cr, Cu/Zn, Ni/Co), offshore distance or water depth (Fe/Mn, Mn/Ti, Co/Ti), paleosalinity (B, Li, Ni, Sr, B/Ga, Sr/Ba, Na/Ca), sedimentary facies ($T_{V+Ni+Cu}$); (2) climatic type, including temperature and humidity (Rb/Sr, Sr/Cu, Mg/Ca, Al/Mg); (3) tectonic type (V/Sc). In practice, a given geochemical indicator may reflect more than one type of environmental information. For example, a fluctuation in the Fe/Mn ratio can indicate a variation in salinity, offshore distance, water depth, or climate [7,23].

The sedimentary environment is a system formed by the close relationships of different environmental factors, so different geochemical indexes in the same environment have significant internal relationships [23]. For example, under an arid climate, the sedimentary environment is characterized by intense oxidation, shallow water, low biological yields,

high salinity, and obvious temperature effects. However, under a humid climate, it is characterized by weak oxidation, deep water, high biological yields, low salinity, and negligible temperature effects. Based on different geochemical indexes such as Sr/Ba, V/Cr, and Ni/Co, Liang et al. (2020) indicate that, from the Shiguai Group to the Daqingshan Formation of the Jurassic in the Shiguai Basin of the Inner Mongolia Autonomous Region, the warm and wet climate gradually changes to a semi-dry and hot climate, the water body becomes shallow, the salinity increases, and the oxidation is enhanced [24]. To improve the accuracy of the prediction of the sedimentary environment using sedimentary geochemical methods, the following aspects need to be further explored [8,10,25]: (1) it is necessary to develop new technology methods to finely analyze sedimentary geochemical information; (2) the methods of using isotopic age to constrain other sedimentary geochemical indicators need to be improved and innovated; (3) quantitative simulation of geochemical process is required; (4) the reference baselines and distribution patterns of sedimentary geochemistry at a larger time (such as era, period) and space scale (such as country) must be established.

The Liaodongwan Depression is rich in oil and gas resources, with the reserves accounting for more than 30% in the Bohai Bay Basin, and the Neogene Guantao Formation is one of the most important hydrocarbon reservoirs [26]. The sedimentary characteristics are not clear, which is one of the main reasons for the lesser discovery of oil and gas fields of the Liaodong sub-uplift, which is a subtectonic unit of the Liaodongwan Depression [26]. Most of the research on the sedimentary environment of the Guantao Formation in the Liaodongwan Depression is carried out by sedimentological, paleontological, logging, and seismic methods, and few studies are based on sedimentary geochemistry. There are two viewpoints on the sedimentary environment of the Neogene Guantao Formation in the Liaodong sub-uplift. One is that it is mainly alluvial fan and braided river, lacking the delta and lake deposits [26–30]; the other is that the lake and lake delta (or braided river delta) deposits are widely distributed [29,31]. The research results on the sedimentary environment of the Guantao Formation based on sedimentary geochemistry mainly come from the adjacent area, and these studies often use sedimentary geochemistry as an auxiliary method to obtain some environmental parameters, such as provenance in the western Bohai Bay Basin [32], paleowater depth in the Bozhong Depression [33], paleoclimate in the Huanghua Depression [34], and paleosalinity, redox, and paleoclimate in the Jizhong Depression [35]. According to Rb/K, V, Al, Ni, and Ga, Pan et al. (2019) recognized that the Guantao Formation in the Bozhong Depression was deposited in a shallow lake gentle slope and identified three transgressions [34], which approximately accord with shallow water sedimentation [27,30]. Li et al. (2019) discovered that the climate successively exhibits hot, cold, and hot characteristics from the Upper, Middle, and Lower Members of the Guantao Formation in the western Bohai Bay Basin according to Sr/Cu, Rb/Sr, and the chemical index of alteration (CIA) [32], and Zhong et al. (2017) reached a similar conclusion in the Liaodongwan Depression with their plant palynology analysis. Therefore, the sedimentary geochemistry research of the adjacent areas could be used as a reference for the study of the paleoclimate and paleoenvironment in the Liaodong Depression [28]. Therefore, based on the data of trace elements and isotopes, combined with whole-rock mineral and clay mineral analyses, this paper aims to reconstruct the sedimentary environment of the Neogene Guantao Formation in the Liaodong sub-uplift via sedimentary geochemistry methods, and it clarifies the characteristics of the sedimentary environment, so as to provide a theoretical basis for oil and gas exploration of the Neogene in the Bohai Bay Basin.

2. Geological Background

The Liaodong sub-uplift is located in the northeast of the Liaodongwan Depression in the Bohai Bay Basin (Figure 1a–c), adjacent to the Liaohe Depression in the northeast and close to the Bozhong Sag and the Bodong Sag in the southwest [28]. It is a favorable area for hydrocarbon migration and has good accumulation conditions [26,36]. The Liaodongwan Depression evolved from a back-arc basin corresponding to the synrift stage during the Mesozoic to an intra-craton rift basin corresponding to the post-rift stage in the Ceno-

zoic [37,38]. The provenance of the Neogene in the Liaodongwan Depression is mainly from the intermediate–acidic magmatic rocks of the Yanshan Mountain and Liaodong uplift [38,39]. The Neogene of the Liaodong sub-uplift is divided into the Guantao Formation (N_1g) and Minghuazhen Formation ($N_{1-2}m$) from bottom to top (Figure 1d). The Guantao Formation, with a thickness of 250−1000 m, can be divided into three members, i.e., the Upper, Middle, and Lower Members (Figure 1d), which are mainly composed of light gray and gray–white sandstones and gravel-bearing sandstones, intercalating or interbedding with thin gray–green, gray–white, and gray mudstones with a single layer thickness of 1–30 m (generally between 2 m and 10 m). During the Neogene, the Liaodongwan Depression subsided intensely (Figure 1e), which benefits organic maturation, and the fault system is dominated by strike−slip faults and normal faults, but the fault activity is weaker than that of the Paleogene [26,32]. The hydrocarbon originated from the Paleogene Shahejie Formation and Dongying Formation of the Liaozhong Sag could migrate to the Neogene Guantao Formation of the Liaodong sub-uplift through the faults [28].

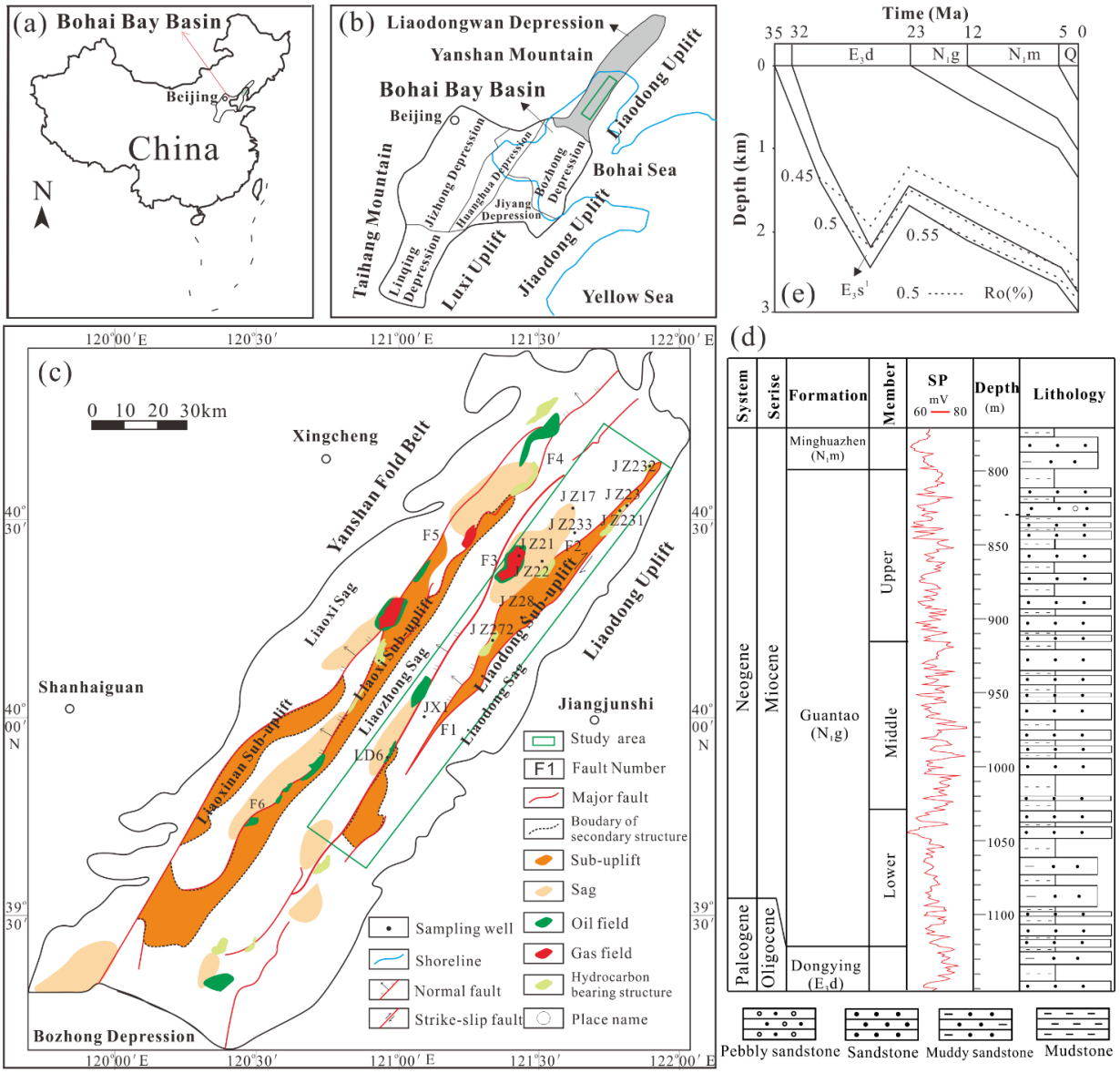

Figure 1. (**a**) Sketch map showing the location of the Bohai Bay Basin; (**b**) location of the Liaodongwan Depression in the Bohai Bay Basin; (**c**) tectonic unit divisions of the Liaodong Depression and location

of sampling wells (modified from Zhong, 2017 [28]); (**d**) composite column of the Guantao Formation (well JZ27); (**e**) burial and thermal history of the Neogene in the study area (modified from Zhang, 2018 [37]), SP: curve of natural potential.

3. Samples and Methods

3.1. Samples

Eighty-four pure mudstone samples of drilling cuttings with a mud logging interval of 5 m or 10 m from 7 wells (Figure 1c) in the Guantao Formation in the Liaodong sub-uplift were selected through careful petrological observation, and the mudstone layers were identified by drilling cuttings and well logging. Sixty-five mudstone samples (collecting one sample in a thin single layer, and 2 or 3 samples in thicker ones) from wells JZ17, JX1, and JZ27 were selected to detect trace elements, among which 12 samples from well JZ17 and JZ27 had a matching isotopic analysis. Twenty-six mudstone samples (collecting 1 sample in a single layer) of wells JZ17, JZ27, and JZ21 had matching carbon, oxygen, and strontium isotope analyses, and to compensate for the insufficient sample quantity, seven samples from JZ23 and five samples from JZ22 were collected for carbon and oxygen isotope and strontium isotope analysis, respectively.

3.2. Methods

To establish the geochemical indexes of provenance, paleoclimate, paleosalinity, paleotemperature, paleodepth, and redox, forty-five elements were considered, including 30 trace elements (Zr, Hf, W, Mo, Ta, Nb, Ti, As, Ba, Be, Bi, Cd, Co, Cr, Cs, Cu, Ga, In, Li, Mn, Ni, Pb, Sr, V, Zn, Sc, Rb, Tl, Th, and U) and 15 rare earth elements (La, Ce, Pr, Nd, Sm, Eu, Gd, Tb, Dy, Ho, Er, Tm, Yb, Lu, and Y) that are not discussed in the study, except that La is used to calculate the paleowater depth. The samples were ground to less than 74 μm in an agate mortar, and then 25 mg of ground sample was fully reacted with a mixed solution of hydrofluoric acid (1 mL) and nitric acid (0.5 mL) in a closed container (constant temperature 185 °C), and then 25 mL solution was introduced into the ICP-AES device ELEMENT XR produced by Thermo Scientific (Waltham, MA, USA), with the relative error less than 10%, following the national standard prepared by Li et al. (2010) [40].

To calculate the paleosalinity and paleotemperature via carbon and oxygen isotopes, thirty-three mudstone samples were pulverized to fine powder (less than 150 μm) in an agate mortar and were reacted with 100% orthophosphoric acid at 25 °C, and the extracted CO_2 was analyzed on a gas-source mass spectrometer MAT252, following the analytical procedure of the petroleum industry standard prepared by Li et al. (2008) [41]. The carbon and oxygen isotope values are reported in per mil to the V-PDB, and the relative standard deviations are less than 0.2‰ and 0.3‰, respectively.

To clarify the sedimentary water nature and weathering degree of the mudstones, thirty-one mudstone samples were ground and repeatedly leached with 0.8 mol/L hydrochloric acid, and pure Sr was separated from the clear solution using a cation exchange column (AG50W-8). The $^{87}Sr/^{86}Sr$ values were measured using the thermal ionization isotope mass spectrometer Triton Plus, according to the analytical process of the national standard prepared by Zhang et al. (1999) [42].

The mineral compositions of mudstones cannot be identified under a polarized microscope. Thus, to analyze the mineralogical characteristics, the whole-rock mineral compositions of eight mudstone samples from wells JZ231 and J232, and the clay mineral compositions of four mudstone samples from well LD6, were analyzed by an X-ray diffraction (XRD) analyzer, D/max-2500, in accordance with the national standard SY/T 5163-2018. The vitrinite reflectance (Ro) of four mudstone samples from wells JZ233 and J272 was measured by microphotometer 641002 following the standard SY/T 5163-2018. The analyses of clay mineral XRD and Ro aimed to determine the diagenetic phase of the mudstones in the Guantao Formation in the study area.

Experiments on trace elements, carbon and oxygen isotopes, and strontium isotopes were carried out by the CNOOC Experimental Center. Data of XRD and Ro were collected from the CNOOC Energy Development Co., Ltd., Tianjin, China.

4. Results

4.1. Mineral Compositions

Quartz (average 40%) is the major mineral of the mudstones of the Guantao Formation in the Liaodong sub-uplift, followed by clay minerals (20.6%), plagioclase (13.25%), and K-feldspar (10.75%), and carbonates are relatively rare (average 3.5%) (Table 1). The clay minerals are dominated by I/S mixed-layer clay mineral (average 73%) (Table 1).

4.2. Trace Elements

According to the significance of element content changing with the sedimentary environment [21–23], 16 trace elements (Table 2) were selected for key analysis, and the interrelationships between every two trace elements are given in Table 3. The content of some trace elements, such as Cr, Ti, Mn, Sr, Zr, Ba, and Rb, had a great range of variation; in particular, Mn varied from 64.19 to 7296.41 μg/g. On average, Ti, Mn, Zr, and Ba in well JX1 were more concentrated than in wells JZ17 and JZ27, and other trace elements were roughly equivalent. The Sr content of the Guantao Formation was in the range of 51.4–249.58 μg/g, with an average value of 122.44 μg/g. The Sr/Cu ratios of the Neogene Guantao Formation were in the range of 2.49–16.05 (mean 7.67). U/Th, V/Cr, and Ni/Co in the Guantao Formation were in the range of 0.13–0.56 (mean 0.23), 0.28–1.80 (mean 0.98), and 1.06–11.30 (mean 2.68), respectively.

4.3. Isotopes

The $\delta^{13}C$ of the Neogene Guantao Formation varied from −17.18‰ to −0.27‰ (mean −10.41‰), and $\delta^{18}O$ ranged from −12.79‰ to −3.85‰ (mean −7.83‰) (Table 4).

The $^{87}Sr/^{86}Sr$ ratios of the Neogene Guantao Formation in the study area ranged from 0.7109 to 0.7218, with an average of 0.7151 (Table 4).

4.4. Geochemical Indicators Used for Reconstruction of the Paleoenvironment and Paleoclimate

Former researchers have presented and used a variety of geochemical compositions, and some geochemical indicators were demonstrated to be more practical. Relative to qualitative geochemical indicators, quantitative ones are widely applied and are more convenient for academic exchange due to their universality in different regions. Jones and Manning (1994) considered DOP (pyrite Fe/total Fe), U/Th, authigenic U, V/Cr, and Ni/Co as the most sensitive indicators for the redox condition by comparing the reliability of several geochemical indexes of ancient mudstones using the factor analysis method [17]. However, some trace and rare earth elements, such as Mo, Cr, V, Ga, and Nb, may have multiple sources, such as detrital inputs, seawater, organic matter, and volcanic activity [21]. Thus, the elements with authigenic origin and a relatively stable nature during burial, which could accurately indicate primary environmental conditions, should be selected to reconstruct the paleoenvironment [13,14]. The relatively reliable trace elements that must be rarely influenced by terrigenous detritus were chosen by correlation analysis (Table 3). Following the above principles, eleven geochemical indicators, such as Sr/Ba, Sr/Cu, and V/Cr (Table 5), were used in the study.

Table 1. XRD analysis data and vitrinite reflectance of mudstones of the Guantao Formation in the Liaodong sub-uplift.

Well	Depth (m)	Content (wt %)																Ro (%)
		Quartz	K-Feldspar	Plagioclase	Calcite	Anhydrite	Ankerite	Clay	Siderite	Total	Illite	Kaolinite	Chlorite	I/S	Total	Smectite in I/S		
JZ231	705	30	16	10	0	1	2	38	3	100								
	735	34	20	6	0	0	3	36	1	100								
	780	31	11	21	0	2	2	33	0	100								
	870	48	8	16	1	1	2	23	1	100								
JZ232	789.10	51	5	8	0	3	0	30	3	100								
	792.20	37	7	13	0	5	0	35	3	100								
	1200	43	12	17	0	0	3	23	2	100								
	1250	46	7	15	1	2	1	28	0	100								
LD6	1000										13	8	4	75	100	65		
	1060										11	11	6	72	100	65		
	1110										11	10	4	75	100	60		
	1150										16	9	5	70	100	60		
JZ233	780																	0.28
	1240																	0.30
JZ272	700																	0.36
	1020																	0.41

Note: (1) The samples from JZ232 were collected from the drilling core; other samples were drilling cuttings. (2) I/S represents mixed-layer clay mineral.

Table 2. Data of trace elements and La in the mudstones of the Guantao Formation.

Well	Depth (m)	Color of Mudstone	Content (μg/g)																Elemental Ratios						
			La	Li	Cr	Ti	V	Mn	Co	Ni	Cu	Zn	Ga	Sr	Zr	Ba	Rb	Th	U	Sr/Ba	Mn/Ti	V/Cr	Ni/Co	U/Th	Sr/Cu	Rb/Sr
JZ17	935	green gray	27.35	46.75	84.59	5918.24	99.23	129.01	15.45	18.65	7.19	184.18	26.10	110.92	199.46	690.07	241.19	9.00	3.48	0.16	0.02	1.17	1.21	0.39	15.43	2.17
JZ17	945	green gray	14.07	40.79	55.88	2325.66	52.53	85.29	6.38	18.14	9.94	73.26	18.61	51.40	150.05	294.63	72.63	4.55	2.29	0.17	0.04	0.94	2.84	0.50	5.17	1.41
JZ17	955	green gray	33.81	49.64	104.49	3924.17	112.55	772.63	16.73	40.84	20.31	109.28	26.50	110.28	161.90	694.45	194.05	13.07	3.56	0.16	0.20	1.08	2.44	0.27	5.43	1.76

Table 2. *Cont.*

Well	Depth (m)	Color of Mudstone	Content (μg/g)																Elemental Ratios						
			La	Li	Cr	Ti	V	Mn	Co	Ni	Cu	Zn	Ga	Sr	Zr	Ba	Rb	Th	U	Sr/Ba	Mn/Ti	V/Cr	Ni/Co	U/Th	Sr/Cu	Rb/Sr
JZ17	970	green gray	40.86	60.02	97.07	3950.78	117.53	450.98	15.25	29.77	29.32	116.35	27.80	111.27	142.78	775.95	216.58	15.23	3.95	0.14	0.11	1.21	1.95	0.26	3.80	1.95
JZ17	990	green gray	21.51	42.78	136.74	4031.68	106.99	455.56	15.53	36.46	25.67	104.31	21.79	81.33	163.35	476.91	145.67	11.08	3.52	0.17	0.11	0.78	2.35	0.32	3.17	1.79
JZ17	1015	green gray	63.67	59.42	145.43	5355.98	102.35	175.24	13.42	33.15	13.29	112.23	22.80	169.82	229.73	785.65	150.04	16.92	2.87	0.22	0.03	0.70	2.47	0.17	12.77	0.88
JZ17	1030	green gray	40.53	50.10	78.21	5162.29	90.53	100.98	5.61	17.71	19.58	85.10	23.83	155.44	221.41	910.15	177.24	12.39	3.61	0.17	0.02	1.16	3.16	0.29	7.94	1.14
JZ17	1040	green gray	35.62	51.69	163.91	4350.30	113.95	197.59	17.33	53.63	20.47	118.36	25.77	101.29	144.48	719.11	215.27	13.66	7.65	0.14	0.05	0.70	3.09	0.56	4.95	2.13
JZ17	1050	green gray	54.76	39.69	298.58	5188.36	82.34	510.54	11.29	98.63	11.16	109.10	23.36	179.21	185.45	709.56	201.51	13.88	2.75	0.25	0.10	0.28	8.73	0.20	16.05	1.12
JZ17	1065	green gray	43.69	53.57	192.21	6303.40	113.77	206.09	14.72	29.93	17.12	144.06	24.29	249.58	380.58	984.92	247.87	14.86	3.53	0.25	0.03	0.59	2.03	0.24	14.58	0.99
JZ17	1080	green gray	17.27	32.67	150.56	4716.56	105.78	119.70	3.94	21.29	13.81	65.53	17.73	133.66	220.91	605.10	134.54	11.95	1.85	0.22	0.03	0.70	5.40	0.15	9.68	1.01
JZ17	1095	green gray	30.66	30.70	151.12	5540.33	90.48	175.06	12.81	40.10	18.70	113.20	20.58	193.06	281.99	808.75	159.67	14.96	2.39	0.24	0.03	0.60	3.13	0.16	10.33	0.83
JZ17	1110	green gray	30.26	35.13	61.89	3831.49	76.34	154.17	11.25	20.81	17.27	84.09	19.00	168.43	145.00	640.22	139.35	10.88	2.10	0.26	0.04	1.23	1.85	0.19	9.75	0.83
JZ17	1125	green gray	41.69	34.29	87.58	4461.03	85.17	211.76	12.59	29.44	22.86	102.94	18.80	75.83	143.62	479.14	152.83	11.86	3.33	0.16	0.05	0.97	2.34	0.28	3.32	2.02
JZ17	1140	green gray	29.13	30.56	123.24	4048.02	65.62	72.40	7.49	35.66	10.71	69.09	15.49	64.98	153.09	431.34	123.00	8.22	2.32	0.15	0.02	0.53	4.76	0.28	6.07	1.89
JZ17	1150	gray	33.41	33.32	72.59	4331.95	69.89	144.13		73.48	18.06	94.53	20.74	219.89	226.77	891.08	143.60	12.04	4.48	0.25	0.03	0.96	0.61	0.37	12.18	0.65
JZ17	1170	gray	37.14	37.38	94.35	4865.80	94.87	198.15	11.96	28.43	22.21	103.92	21.87	108.11	198.20	648.73	176.17	12.52	3.12	0.17	0.04	1.01	2.38	0.25	4.87	1.63
JZ17	1190	gray	28.48	31.84	72.36	3385.51	71.07	189.36	7.44	17.07	13.16	67.56	15.16	150.84	149.92	1416.95	119.63	7.56	1.79	0.11	0.06	0.98	2.29	0.24	11.46	0.79
JZ17	1200	gray	35.55	32.18	77.90	3720.42	88.92	132.17	12.34	27.69	21.18	82.22	18.15	71.37	132.17	503.83	146.08	9.42	2.53	0.14	0.04	1.14	2.24	0.27	3.37	2.05
JZ17	1210	gray	28.53	29.86	76.42	3529.61	77.54	145.48	9.22	22.18	15.92	78.21	16.08	63.50	114.11	481.27	117.72	8.91	2.21	0.13	0.04	1.01	2.40	0.25	3.99	1.85
JZ17	1225	gray	27.18	37.81	64.91	3287.00	81.53	859.81	10.15	20.06	12.17	78.86	17.48	78.15	97.87	436.78	143.71	9.34	2.48	0.18	0.26	1.26	1.98	0.27	6.42	1.84
JZ17	1240	gray	27.49	25.99	69.47	3003.72	61.43	191.40	6.36	10.13	14.07	64.15	12.15	69.24	128.16	470.58	113.28	7.38	1.68	0.15	0.06	0.88	1.59	0.23	4.92	1.64
JZ17	1255	gray	33.15	27.67	76.19	2443.91	70.31	800.32	8.24	12.38	12.34	71.87	13.00	68.06	115.04	476.51	111.18	7.92	2.05	0.14	0.33	0.92	1.50	0.26	5.51	1.63
JZ17	1280	gray	59.26	61.86	115.89	6245.56	132.71	175.01	8.92	29.16	34.40	113.60	28.86	190.49	212.87	1402.85	205.05	15.63	6.22	0.14	0.03	1.15	3.27	0.40	5.54	1.08
JZ17	1300	gray	32.65	35.39	65.04	4467.65	92.68	572.56	13.71	29.24	23.99	102.60	19.22	149.76	151.73	1542.05	129.78	8.89	1.76	0.10	0.13	1.42	2.13	0.20	6.24	0.87
JX1	840	green–gray	30.73	35.28	95.97	7522.14	100.89	82.56	7.05	16.95	15.87	100.90	16.19	90.30	248.41	665.99	134.34	11.02	1.73	0.14	0.01	1.05	2.41	0.16	5.69	1.49
JX1	850	green–gray	56.07	28.04	60.28	7639.95	108.61	134.08	9.37	21.07	14.58	107.00	21.69	115.28	210.59	1146.96	140.16	13.36	2.34	0.10	0.02	1.80	2.25	0.18	7.91	1.22
JX1	880	green–gray	56.56	27.54	111.48	7295.05	121.97	83.35	7.14	21.90	12.76	96.13	17.94	89.43	238.72	659.42	137.63	13.27	1.85	0.14	0.01	1.09	3.07	0.14	7.01	1.54
JX1	900	green–gray	47.17	26.03	84.87	8329.65	119.54	163.04	13.29	33.95	21.01	159.21	21.25	143.84	247.78	2492.65	153.10	12.19	2.13	0.06	0.02	1.41	2.56	0.17	6.84	1.06

Table 2. *Cont.*

Well	Depth (m)	Color of Mudstone	Content (μg/g)																Elemental Ratios						
			La	Li	Cr	Ti	V	Mn	Co	Ni	Cu	Zn	Ga	Sr	Zr	Ba	Rb	Th	U	Sr/Ba	Mn/Ti	V/Cr	Ni/Co	U/Th	Sr/Cu	Rb/Sr
JX1	910	green–gray		25.91	105.23	6799.49	106.40	71.01	5.96	17.61	10.75	91.37	18.08	82.08	290.48	461.33	123.05	11.60	2.08	0.18	0.01	1.01	2.95	0.18	7.64	1.50
JX1	920	green–gray	31.51	34.44	100.83	7996.19	94.25	93.75	15.05	21.63	14.42	115.40	14.12	122.75	320.02	1176.62	124.51	10.08	2.11	0.10	0.01	0.93	1.44	0.21	8.51	1.01
JX1	935	green–gray	31.51	33.27	123.70	7389.68	101.99	109.72	15.33	24.19	17.37	118.91	13.47	136.92	304.81	2822.68	123.44	8.37	1.81	0.05	0.01	0.82	1.58	0.22	7.88	0.90
JX1	945	green–gray	37.65	29.72	117.16	7807.64	118.53	191.11	13.89	20.27	20.61	118.62	16.37	125.50	267.23	523.59	117.17	10.23	1.94	0.24	0.02	1.01	1.46	0.19	6.09	0.93
JX1	955	green–gray	38.79	27.30	94.84	7592.64	108.14	113.84	10.94	19.36	17.82	144.13	16.23	106.64	246.08	716.54	123.74	10.25	1.84	0.15	0.01	1.14	1.77	0.18	5.99	1.16
JX1	960	green–gray	36.78	23.64	56.69	7378.96	91.43	467.04	14.92	24.10	21.69	139.71	16.91	214.62	298.53		113.13	8.12	1.58		0.06	1.61	1.62	0.19	9.90	0.53
JX1	975	green–gray	48.20	24.23	60.72	7599.61	99.02	153.92	10.21	23.30	18.07	143.29	19.07	136.31	222.54	1698.38	150.68	12.22	2.03	0.08	0.02	1.63	2.28	0.17	7.54	1.11
JX1	985	green–gray	31.28	29.08	62.11	10,324.30	107.83	225.85	23.53	24.97	20.63	126.92	19.23	126.83	276.47	725.80	140.98	14.29	2.45	0.17	0.02	1.74	1.06	0.17	6.15	1.11
JX1	1005	green–gray	13.63	31.89	98.11	6004.91	104.40	7296.42	6.77	10.21	20.69	79.02	11.00	51.61	123.34	460.70	74.59	6.54	1.54	0.11	1.22	1.06	1.51	0.24	2.49	1.45
JZ27	790	green–gray	44.89	33.08	108.58	5048.29	91.83	432.62	9.49	19.21	11.13	95.95	16.74	55.11	168.36	373.39	114.65	9.85	2.26	0.15	0.09	0.85	2.02	0.23	4.95	2.08
JZ27	800	green–gray	34.97	41.12	148.07	5887.82	114.40	289.23	9.07	19.65	14.37	101.32	17.98	84.44	211.71	418.13	133.73	10.91	2.22	0.20	0.05	0.77	2.17	0.20	5.88	1.58
JZ27	810	green–gray	31.63	38.78	129.87	5479.04	118.69	323.97	10.86	23.07	21.40	110.27	18.23	80.08	172.03	405.36	132.57	10.67	2.29	0.20	0.06	0.91	2.12	0.21	3.74	1.66
JZ27	830	gray–white	37.14	31.28	107.89	5757.83	101.67	270.11	11.83	21.33	21.93	122.00	18.33	86.78	221.86	423.03	130.63	11.33	2.48	0.21	0.05	0.94	1.80	0.22	3.96	1.51
JZ27	840	gray–white	28.82	36.43	76.08	5383.18	86.10	109.06	8.26	20.44	17.77	90.06	21.19	103.20	164.45	433.72	139.02	12.75	1.60	0.24	0.02	1.13	2.47	0.13	5.81	1.35
JZ27	850	gray–white	54.53	46.87	80.06	5883.38	96.68	371.80	9.27	25.26	16.62	106.14	22.56	114.18	174.83	339.73	138.72	13.40	2.11	0.34	0.06	1.21	2.72	0.16	6.87	1.21
JZ27	860	gray–white	6.23	6.26	136.47	1827.68	87.40	274.00	3.57	15.24	13.87	83.81	4.20	208.95	82.70	129.43	3.99	3.47	1.03		0.15	0.64	4.27	0.30	15.07	0.02
JZ27	870	gray–white	20.84	25.06	63.93	3516.57	70.65	769.28	10.38	20.57	16.03	93.74	16.33	76.41	179.97	316.39	84.39	7.56	1.63	0.24	0.22	1.11	1.98	0.22	4.77	1.10
JZ27	880	gray–white	45.05	34.00	101.83	5562.51	94.51	674.77	14.35	24.29	17.64	131.78	18.37	83.43	194.36	392.05	122.74	10.28	2.34	0.21	0.12	0.93	1.69	0.23	4.73	1.47
JZ27	890	gray–white	49.71	30.80	181.46	5424.03	105.79	915.57	14.20	59.34	29.03	125.94	20.15	96.90	167.23	385.74	129.42	11.98	2.94	0.25	0.17	0.58	4.18	0.25	3.34	1.34
JZ27	900	gray–white	32.56	34.51	114.79	5746.42	108.16	644.67	13.42	28.81	24.20	114.79	18.04	86.56	172.05	412.08	125.96	9.77	2.47	0.21	0.11	0.94	2.15	0.25	3.58	1.46
JZ27	920	gray–white	22.10	28.92	82.17	5338.33	100.44	523.44	24.90	57.80	22.66	112.94	18.24	69.61	168.98	338.55	119.39	10.09	2.33	0.21	0.10	1.22	2.32	0.23	3.07	1.72
JZ27	930	gray–white	22.04	27.77	167.98	4942.67	90.04	74.19	4.71	53.25	11.18	72.27	19.63	132.89	176.95	394.25	97.09	9.88	1.30	0.34	0.02	0.54	11.30	0.13	11.89	0.73
JZ27	940	gray–white	39.95	27.26	107.42	5777.01	86.82	180.83	10.59	21.82	12.54	106.24	17.10	150.87	220.01	655.91	121.23	11.01	2.14	0.23	0.03	0.81	2.06	0.19	12.03	0.80
JZ27	950	gray–white	27.02	28.12	77.22	7389.18	78.34	95.65	4.15	14.23	10.94	88.25	15.57	142.45	235.12	455.53	123.93	9.62	1.92	0.31	0.01	1.01	3.43	0.20	13.02	0.87

Table 2. *Cont.*

Well	Depth (m)	Color of Mudstone	Content (μg/g)																Elemental Ratios						
			La	Li	Cr	Ti	V	Mn	Co	Ni	Cu	Zn	Ga	Sr	Zr	Ba	Rb	Th	U	Sr/Ba	Mn/Ti	V/Cr	Ni/Co	U/Th	Sr/Cu	Rb/Sr
JZ27	960	gray–white	32.13	38.32	94.47	6234.04	91.89	165.39	7.85	23.30	9.58	102.19	19.53	128.39	197.12	731.40	126.72	9.76	1.64	0.18	0.03	0.97	2.97	0.17	13.41	0.99
JZ27	970	gray–white	34.40	26.88	93.96	6482.61	87.96	316.92	9.06	19.96	24.39	87.29	14.52	108.62	246.76	430.71	117.32	9.46	1.96	0.25	0.05	0.94	2.20	0.21	4.45	1.08
JZ27	980	gray–white	31.66	25.97	101.58	6598.86	78.17	409.60	10.44	21.99	11.75	93.84	14.36	108.67	244.85	353.02	128.98	10.26	1.69	0.31	0.06	0.77	2.11	0.16	9.25	1.19
JZ27	1000	gray–white	35.51	35.17	81.81	6438.02	102.53	863.41	15.41	35.90	27.22	124.74	18.13	144.91	222.38	739.40	115.10	8.33	2.03	0.20	0.13	1.25	2.33	0.24	5.32	0.79
JZ27	1020	gray–white	23.57	24.92	112.42	6244.57	90.44	332.41	8.12	27.95	15.12	84.01	14.53	132.90	268.72	769.09	108.32	8.40	1.68	0.17	0.05	0.80	3.44	0.20	8.79	0.82
JZ27	1030	gray–white	34.57	43.80	96.91	5439.39	121.25	1230.44	17.44	45.34	16.70	110.75	20.57	152.14	150.53	404.28	115.77	10.27	2.14	0.38	0.23	1.25	2.60	0.21	9.11	0.76
JZ27	1050	gray–white	28.77	32.58	101.26	5071.25	91.67	164.76	21.86	44.09	18.39	104.06	18.57	136.69	215.98	1205.74	141.58	9.94	1.98	0.11	0.03	0.91	2.02	0.20	7.43	1.04
JZ27	1060	gray–white	22.56	26.57	156.47	6684.99	90.40	64.19	5.74	24.67	9.98	84.78	12.65	153.64	231.65	539.12	66.99	7.17	1.37	0.28	0.01	0.58	4.29	0.19	15.39	0.44
JZ27	1070	gray–white	34.65	27.24	267.15	6105.84	93.15	498.41	13.73	26.43	16.78	103.40	14.62	128.09	209.26	490.63	112.57	8.53	1.77	0.26	0.08	0.35	1.92	0.21	7.63	0.88
JZ27	1080	gray–white		22.70	112.43	6483.42	104.99	129.66	8.93	29.22	30.52	112.44	19.56	133.38	236.50	1669.39	134.51	10.03	1.80	0.08	0.02	0.93	3.27	0.18	4.37	1.01
JZ27	1100	gray–white	27.77	22.38	93.31	5673.14	85.73	1164.23	18.77	36.31	14.16	92.83	12.81	181.35	240.61	855.87	67.73	6.01	1.29	0.21	0.21	0.92	1.93	0.21	12.81	0.37
JZ27	1115	gray–white	48.52	20.53	98.45	5075.88	90.51	123.91	18.06	39.44	13.47	118.03	16.44	209.96	171.16	1467.54	113.08	7.60	1.40	0.14	0.02	0.92	2.18	0.18	15.59	0.54
JZ17		Min.	14.07	25.99	55.88	2443.91	61.43	72.40	3.94	10.13	10.71	64.15	12.15	63.50	97.87	431.34	72.63	7.38	1.68	0.10	0.02	0.28	0.61	0.15	3.17	0.65
		Max.	63.67	61.86	298.58	6303.40	132.71	859.81	17.33	98.63	34.40	144.06	28.86	249.58	380.58	1542.05	247.87	16.92	7.65	0.26	0.33	1.42	8.73	0.56	16.05	2.17
		Avg.	34.71	39.72	108.67	4373.70	90.54	283.57	10.93	32.56	18.52	94.63	20.18	129.70	179.06	754.43	159.10	11.61	3.10	0.17	0.08	0.94	2.73	0.28	7.72	1.44
JX1		Min.	13.63	23.64	56.69	6004.91	91.43	71.01	5.96	10.21	10.75	79.02	11.00	51.61	123.34	460.70	74.59	6.54	1.54	0.05	0.01	0.82	1.06	0.14	2.49	0.53
		Max.	56.56	35.28	123.70	10,324.30	221.97	7296.41	23.53	33.95	21.69	159.21	21.69	214.62	320.02	2822.68	153.10	14.29	2.45	0.24	1.22	1.80	3.07	0.24	9.90	1.54
		Avg.	38.32	28.95	90.15	7667.71	106.38	706.59	11.80	21.50	17.40	118.51	17.04	118.62	253.46	1129.22	127.43	10.89	1.96	0.13	0.11	1.26	2.00	0.18	6.90	1.15
JZ27		Min.	6.26	63.93	1827.68	70.65	64.19	3.57	14.23	9.58	72.27	4.20	55.11	82.70	129.43	3.99	3.47	1.03	6.23	0.05	0.01	0.82	1.06	0.14	2.49	0.53
		Max.	54.53	46.87	267.15	7389.18	121.25	1230.44	24.90	59.34	30.52	131.78	22.56	209.96	268.72	1669.39	141.58	13.40	2.94	0.38	0.23	1.25	11.30	0.30	15.59	2.08
		Avg.	32.75	30.27	114.59	5610.96	94.82	422.69	11.65	29.59	17.38	102.74	17.00	121.87	198.00	575.17	113.56	9.57	1.92	0.23	0.08	0.90	2.89	0.20	8.01	1.07
Guantao Formation		Min.	6.23	6.26	55.88	1827.68	61.43	64.19	3.57	10.13	9.58	64.15	4.20	51.61	82.70	129.43	3.99	3.47	1.03	0.05	0.01	0.28	0.61	0.13	2.49	0.02
		Max.	63.67	61.86	298.58	10,324.30	132.71	7296.41	24.90	98.63	34.40	159.21	28.86	249.58	380.58	2822.68	247.87	16.92	7.65	0.38	1.22	1.80	11.30	0.56	16.05	2.17
		Avg.	34.59	33.35	107.43	5603.18	95.73	432.85	11.43	28.95	17.79	103.17	18.14	123.97	202.91	748.81	133.85	10.57	2.35	0.19	0.08	0.98	2.65	0.23	7.67	1.23

Table 2. *Cont.*

Well	Depth (m)	Color of Mudstone	Content (μg/g)																Elemental Ratios						
			La	Li	Cr	Ti	V	Mn	Co	Ni	Cu	Zn	Ga	Sr	Zr	Ba	Rb	Th	U	Sr/Ba	Mn/Ti	V/Cr	Ni/Co	U/Th	Sr/Cu	Rb/Sr
Average marine mudstone		Avg.	10.00	57.00	90.00	4600.00	120.00	6700.00	74.00	225.00	250.00	165.00	20.00	180.00	150.00	2300.00	80.00	7.00	1.30	595.00	0.08	1.46	1.33	3.04	0.19	0.72
Basic magmatic rock		Avg	25.00	10.00	223.00	7820.00	230.00	1260.00	46.00	100.00	58.00	104.00	18.70	570.00	120.00	450.00	36.00	2.80	0.70	388.00	1.27	0.16	1.03	2.17	0.25	9.83
Intermediate-acidic magmatic rock		Avg	35.00	20.00	44.00	2900.00	67.00	320.00	12.00	19.00	18.50	60.00	18.70	405.00	165.00	850.00	18.00	9.00	1.50	104.50	0.48	0.11	1.52	1.58	0.17	21.89
Acidic magmatic rock		Avg.	41.00	19.00	6.60	1380.00	23.00	380.00	3.00	5.20	5.50	40.00	18.00	220.00	155.00	680.00	26.00	17.00	2.90	33.70	0.32	0.28	3.48	1.73	0.17	40.00
Upper crust of Eastern China		Avg.	33.00	20.00	44.00	3070.00	70.00	600.00	12.00	21.00	17.00	63.00	18.00	300.00	170.00	640.00	18.00	9.50	1.80	108.00	0.47	0.20	1.59	1.75	0.19	17.65
Mudstone of Eastern China		Avg.	50.00	38.00	72.00	4560.00	115.00	460.00	14.00	34.00	29.00	80.00	20.50	110.00	210.00	590.00	23.00	14.00	3.10	178.00	0.19	0.10	1.60	2.43	0.22	3.79
Average mudstone		Avg.	92.00	66.00	90.00	4600.00	130.00	850.00	19.00	68.00	45.00	95.00	19.00	300.00	160.00	580.00	20.00	12.00	3.70	243.00	0.52	0.18	1.44	3.58	0.31	6.67

Note: (1) All the samples are drilling cuttings. (2) Data of the average marine mudstone and the average mudstone are quoted from Turekian and Wedepohl (1961) [43]. Data of the upper crust and the magmatic rock of Eastern China are quoted from Yan (1997) [44].

Table 3. Correlation coefficients of trace elements in the mudstones of the Guantao Formation.

	Li	Cr	Ti	V	Mn	Co	Ni	Cu	Zn	Ga	Sr	Zr	Ba	Rb	Th	U
Li	1															
Cr	0.13	1														
Ti	−0.10	0.03	1													
V	0.36	0.22	0.52	1												
Mn	−0.01	−0.02	−0.03	0.09	1											
Co	0.18	0.00	0.20	0.31	−0.01	1										
Ni	0.16	0.49	−0.08	0.06	−0.08	0.44	1									
Cu	0.24	−0.05	0.10	0.48	0.13	0.35	0.16	1								
Zn	0.20	0.07	0.54	0.56	−0.11	0.56	0.17	0.29	1							
Ga	0.79	0.09	0.06	0.43	−0.22	0.29	0.39	0.34	0.44	1						
Sr	0.02	0.22	0.18	0.09	−0.21	0.14	0.31	0.04	0.26	0.13	1					
Zr	−0.02	0.15	0.76	0.30	−0.24	0.16	−0.02	0.00	0.43	0.07	0.43	1				
Ba	0.02	−0.09	0.35	0.23	−0.14	0.21	0.07	0.20	0.37	0.15	0.40	0.38	1			
Rb	0.72	0.17	0.12	0.38	−0.22	0.29	0.28	0.25	0.48	0.85	0.14	0.20	0.23	1		
Th	0.61	0.22	0.31	0.53	−0.23	0.20	0.31	0.31	0.35	0.77	0.17	0.30	0.14	0.75	1	
U	0.69	0.14	−0.13	0.32	−0.11	0.25	0.34	0.39	0.25	0.70	0.06	−0.07	0.05	0.70	0.56	1

Table 4. Data of carbon, oxygen, and strontium isotopes in the mudstones of the Guantao Formation.

Well	Depth (m)	Color of Mudstone	$\delta^{13}C$ (‰)	$\delta^{18}O$ (‰)	$^{87}Sr/^{86}Sr$	Parallel Sample of Trace Elements in Table 3 (Yes or No)
JZ17	945	green–gray	−13.10	−9.04	0.7218	Yes
JZ17	1030	green–gray	−7.96	−11.37	0.7203	Yes
JZ17	1095	green–gray	−17.18	−10.53	0.7185	Yes
JZ17	1140	green–gray	−7.75	−11.58	0.7198	Yes
JZ17	1190	green–gray	−8.43	−4.53	0.7169	Yes
JZ17	1280	green–gray	−12.19	−6.65	0.7173	Yes
JZ27	800	gray–white	−12.63	−5.56	0.7125	Yes
JZ27	840	gray–white	−13.02	−7.65	0.7159	Yes
JZ27	890	gray–white	−11.84	−5.10	0.7147	Yes
JZ27	910	gray–white	−8.62	−8.70	0.7163	
JZ27	970	gray–white	−12.46	−6.15	0.7145	Yes
JZ27	1010	gray–white	−8.41	−6.25	0.7126	
JZ27	1050	gray–white	−8.79	−5.80	0.7202	Yes
JZ27	1100	gray–white	−7.30	−5.71	0.7122	Yes
JZ21	1050	gray–white	−7.62	−9.78	0.7109	
JZ21	1090	gray–white	−8.55	−9.08	0.7131	
JZ21	1130	gray–white	−6.75	−9.81	0.7126	
JZ21	1180	gray–white	−0.27	−9.14	0.7127	
JZ21	1200	gray–white	−0.31	−9.08	0.7128	
JZ21	1270	gray–white	−0.82	−5.97	0.7123	
JZ21	1325	gray–white	−12.63	−3.85	0.7122	
JZ28	755	gray–white	−10.86	−5.47	0.7166	

Table 4. *Cont.*

Well	Depth (m)	Color of Mudstone	$\delta^{13}C$ (‰)	$\delta^{18}O$ (‰)	$^{87}Sr/^{86}Sr$	Parallel Sample of Trace Elements in Table 3 (Yes or No)
JZ28	765	gray–white	−11.66	−5.57	0.7164	
JZ28	830	gray–white	−10.23	−5.23	0.7150	
JZ28	860	gray–white	−10.40	−6.02	0.7141	
JZ28	885	gray–white	−11.37	−5.96	0.7144	
JZ22	900	green–gray			0.7138	
JZ22	920	green–gray			0.7133	
JZ22	1120	green–gray			0.7183	
JZ22	1170	green–gray			0.7135	
JZ22	1225	green–gray			0.7135	
JZ23	745	green–gray	−14.49	−12.79		
JZ23	775	green–gray	−13.69	−11.64		
JZ23	825	green–gray	−15.27	−8.18		
JZ23	860	green–gray	−15.32	−8.08		
JZ23	915	green–gray	−14.27	−9.37		
JZ23	960	green–gray	−14.11	−9.14		
JZ23	990	green–gray	−15.38	−9.72		

Note: All the samples are drilling cuttings.

Table 5. Criteria and environmental meanings of geochemical indicators used in the study.

Type	Geochemical Indicator	Criteria	Environmental Information	References
Salinity	Sr/Ba	<0.6	Freshwater or continental	[45]
		0.6–1	Brackish water or transition environment	
		>1	Saline water or marine	
	Sr	100–300 μg/g	Freshwater or continental	
		800–1000 μg/g	Saline water or marine	
	Li	<90 μg/g	Freshwater or continental	[7]
		90–150 μg/g	Brackish water or transition environment	
		>150 μg/g	Saline water or marine	
	Ni	<25 μg/g	Freshwater or continental	[7,22]
		25–40 μg/g	Brackish water or transition environment	
		>40 μg/g	Saline water or marine	

Table 5. *Cont.*

Type	Geochemical Indicator	Criteria	Environmental Information	References
Water depth	Mn/Ti	<0.05	Alluvial plain	[22,46]
		0.05–0.15	Lacustrine delta front, shore shallow lake	
		0.15–0.30	Semi-deep lake, prodelta	
	$T_{V+Ni+Cu}$	<130 μg/g	Fluvial	[23,46,47]
		130–170 μg/g	Shore shallow lake	
		170–190 μg/g	Semi-deep lake	
		>190 μg/g	Deep lake	
Redox	V/Cr	<2	Oxic	[17]
		2–4.25	Dysoxic	
		>4.25	Suboxic + anoxic	
	Ni/Co	<5	Oxic	
		5–7	Dysoxic	
		>7	Suboxic + anoxic	
	U/Th	<0.75	Oxic	
		0.75–1.25	Dysoxic	
		>1.25	Suboxic + anoxic	
Climate	Sr/Cu	1–5	Warm and humid	[15,45]
		5–10	Semi-arid and semi-humid	
		>10	Dry and hot	
Weathering	Rb/Sr	Rb/Sr ratio of average mudstone such as UCC (0.33), PAAS (0.08)	Rb/Sr ratio can be used to identify the degree of weathering and indirectly reflect climate; if it is greater than that of the average mudstone, it suggests relatively intense weathering and a warm humid climate.	[21,48]

5. Discussion

5.1. Validity of Geochemical Indicators for Reconstructing Paleosedimentary Environment

The porosity of mudstone could be completely lost due to mechanical compaction during early burial [49], and the subsequent diagenesis process roughly proceeds in a closed system almost independently of external factors [16]. Thus, compared to coarse-grained clastic rocks, mudstones contain more information about the original sedimentary environment [15,23], so geochemical parameters such as the trace elements and isotopes of the mudstones could be better proxies of the sedimentary environment. The mudstone samples of the study recording near-primary sedimentary geochemical compositions had to satisfy the following criteria: (1) a relatively closed diagenetic system due to rapid burial and weak diagenetic alteration [50]; (2) $\delta^{18}O > -9.65‰$, which is the average $\delta^{18}O$ value of the unchanged freshwater limestones of the Paleogene and Neogene [51]; (3) $\delta^{13}C$ and $\delta^{18}O$ have no correlation [52]; (4) geochemical indexes have no relation with other interfering factors such as temperature and diagenetic alteration [53]. $\delta^{18}O$ ratios are more than −9.65‰ in around 75.8% of the samples from the Guantao Formation in the study area, and there is no correlation between $\delta^{13}C$ and $\delta^{18}O$ (Figure 2). Approximately 84.8% of the samples are located in zone I and only 15.2% are located in zone III of the carbonate origin analysis chart (Figure 2), indicating that the carbonates in the mudstones were mainly formed during syngenesis to eodiagenesis. The migratable elements Li,

Mn, Co, Ni, Cu, and U, which are used as geochemical indicators, weakly correlate with the typical detrital elements Zr and Ti (Table 3), revealing that these elements are quite associated with the sedimentary environment [14]. Additionally, the vitrinite reflectance varying from 0.28–0.41 (mean 0.34) and smectite in I/S more than 70% indicate that the mudstones of the Guantao Formation only evolved up to the eodiagenesis phase [54], implying a relatively weak diagenetic alteration. Therefore, the trace element and isotope data of the mudstone samples in the study most probably record near-primary sedimentary geochemical compositions.

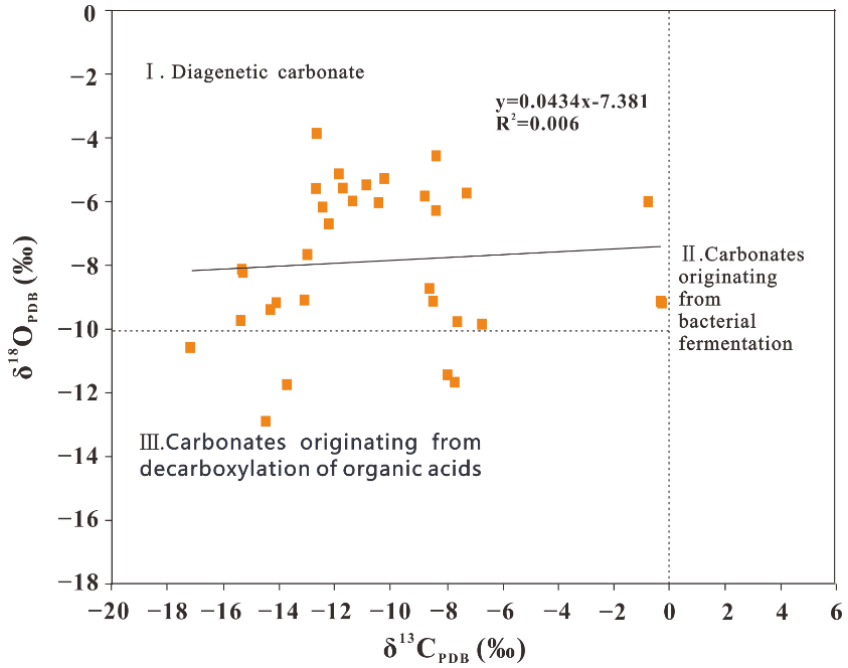

Figure 2. Carbonate origin analysis diagram [55] based on carbon and oxygen isotope values.

5.2. Provenance

The trace element distribution patterns of the mudstones of the Neogene Guantao Formation in the Liaodong sub-uplift are similar to that of the intermediate–acidic magmatic rock in East China (Figure 3), which is generally consistent with the conclusion that the provenance of the Neogene mudstones in the Bohai Bay Basin mainly originates from the intermediate–acidic magmatic rocks of the Yanshanian Period [34,39]. The clay minerals mainly consist of I/S mixed-layer clay mineral and illite, which demonstrates that the source materials are closely associated with the intermediate–acidic magmatic rocks [56]. High concentrations of continental elements Ti, Zr, and Th (Figure 3) and feldspars (K-feldspar + plagioclase, average 24%) represent proximal deposits [14,18,56]. Consequently, the major sediments of the Neogene Guantao Formation in the studied area mainly originated from the intermediate–acidic magmatic rocks of the nearby surrounding uplifts, including Yanashan Mountain and the Liaodong uplift [28], and were precipitated without long-distance transportation.

5.3. Paleoclimate

The richness or loss of some elements and some element ratios can indicate paleoclimate change; for example, Ni, Co, and Zn are higher under a humid climate, and the content of Cu, Sr, and Mn relatively increases in arid conditions [7]. The samples with Sr/Cu ratios in the range of 1–5, 5–10, and >10 (Table 5) account for 29.2%, 47.7%, and 23.1%, respectively (Figure 4a), which shows that the paleoclimate of the Guantao Formation in the study area is mainly semi-arid and semi-humid. In the weathering process, Rb is less able to migrate, while Sr can easily migrate and leach. Therefore, the Rb/Sr ratio can reflect

the weathering intensity and can be used to determine the paleoclimate characteristics further [48]. Rb/Sr ratios of more than 0.32 (the average Rb/Sr ratio 0.32 of the upper crust in Eastern China) and 1.18 (the average Rb/Sr ratio of the mudstones in Eastern China) account for 98.5% and 46.9%, respectively (Figure 4b), which indicates that the provenance area of the Guantao Formation has experienced intense chemical weathering due to the warm and humid climate. Furthermore, the terrigenous clastic supply increases as a result of intense chemical weathering, which causes the $^{87}Sr/^{86}Sr$ ratios to increase in the carbonates of the mudstones [57]. The $^{87}Sr/^{86}Sr$ ratios of the mudstones of the Guantao Formation in the study area are significantly higher than that of the modern river [7] (Figure 5), which further indicates that the chemical weathering was intense and that the climate was warm and humid during the sedimentation period of the Guantao Formation. The paleoclimate of the Guantao Formation in the Liaodong sub-uplift is similar to that deduced by [32] based on elemental indexes, which shows regional climate change consistency.

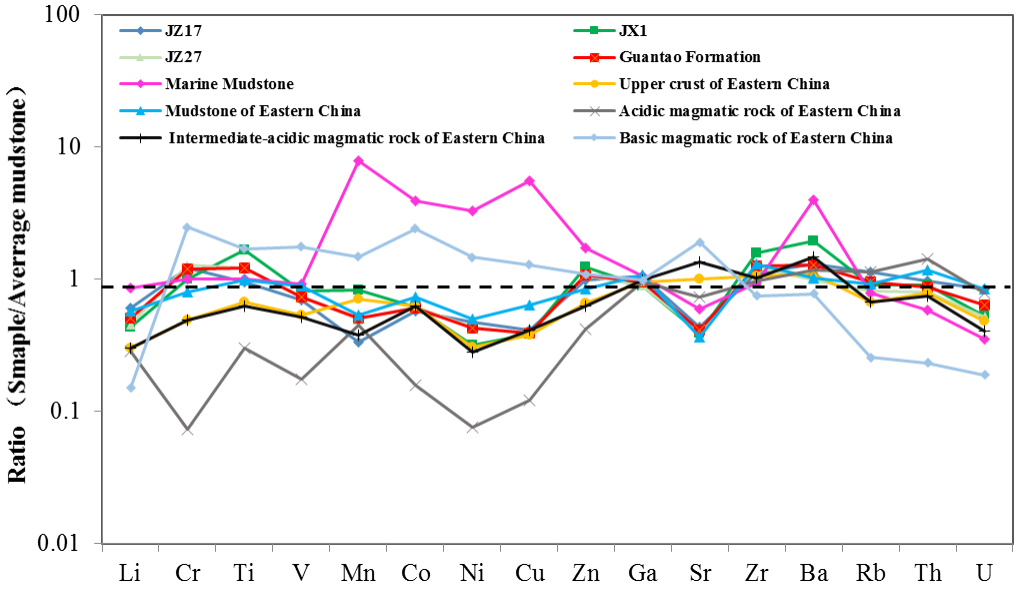

Figure 3. Trace element distribution patterns of the mudstones of the Neogene Guantao Formation in the Liaodong sub-uplift (data are normalized by the average mudstone values listed in Table 2).

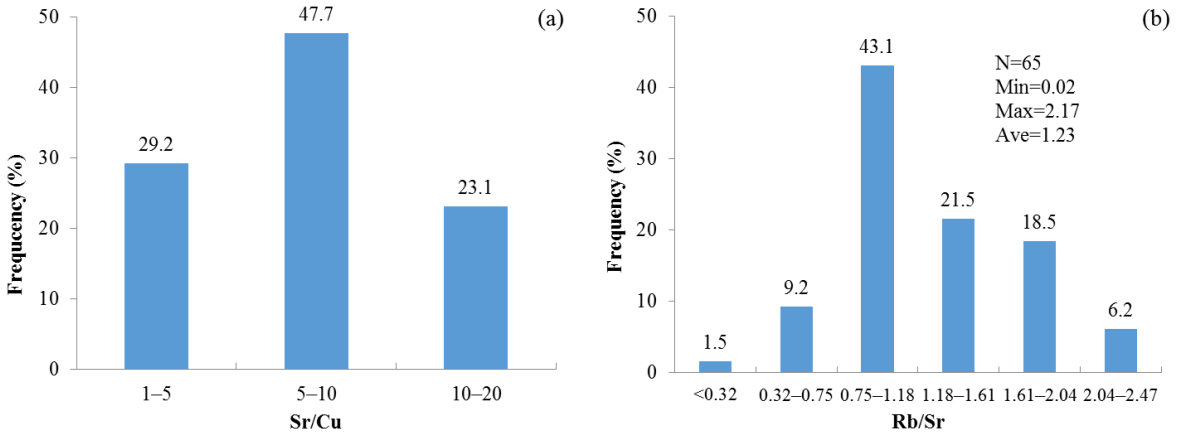

Figure 4. (**a**) Distribution histogram of Sr/Cu ratio. (**b**) Comparison diagram of Rb/Sr ratio of the Guantao Formation with the average marine mudstone and the mudstone of Eastern China.

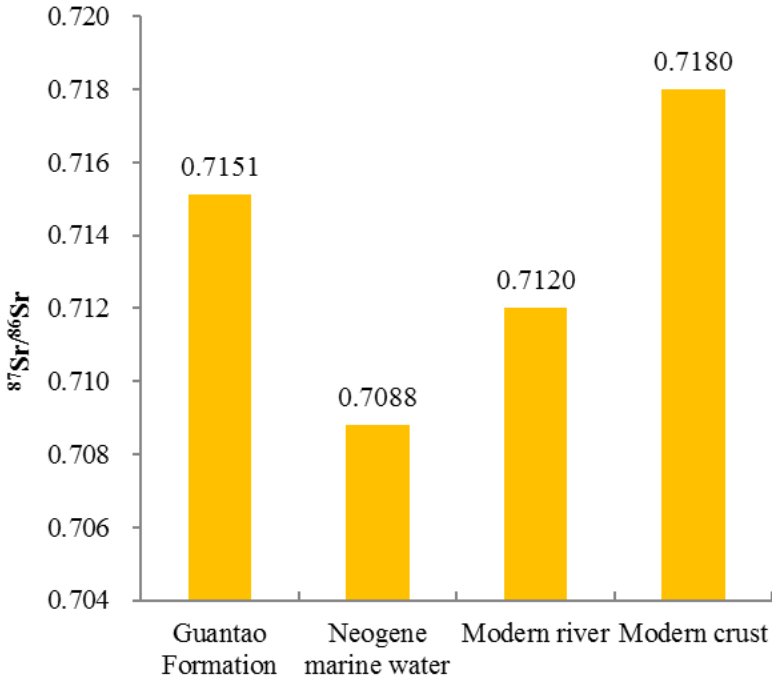

Figure 5. Comparison diagram of $^{87}Sr/^{86}Sr$ ratio of the Guantao Formation with Neogene marine water, modern river and modern crust [7].

5.4. Paleoenvironment

5.4.1. Paleosalinity

The trace element distribution patterns of the mudstones of the Neogene Guantao Formation significantly differ from that of the average marine mudstone, and they resemble that of the average mudstone of Eastern China, but the mudstones contain much lower Li, Mn, Co, Ni, and Cu (Figure 3) content, which are often enriched in a saline sedimentary environment [7]. Thus, the mudstones of the Guantao Formation in the study area are deposited in continental freshwater.

The Sr content and Sr/Ba ratio of sediments are significantly positively correlated with paleosalinity, so they can be used as sensitive identification parameters for paleosalinity [45]. The Sr content (Table 2) of the Guantao Formation is similar to that (<300 μg/g) of freshwater mudstone [58] and approximates that of the mudstone in Eastern China, and the Sr content in 87.7% of the samples is lower than 180 μg/g (Figure 6a), which is the Sr content of the average deep-sea clay [43]. Sr/Ba ratios in the range of 0.05–0.38 (mean 0.19) are less than the upper limit, 0.6, of freshwater sediments [45]. In addition, mudstones of marine (or saline lake) and continental freshwater can also be distinguished according to the content of Li and Ni [7,22,23]. The average content of Li and Ni in the Guantao Formation is significantly lower than that in the marine mudstone, but close to that of the freshwater mudstone (Figure 6c).

Most of the $\delta^{13}C$ and $\delta^{18}O$ values of the Guantao Formation in the study area lie within the ranges of $\delta^{13}C$ (−15–−5‰) and $\delta^{18}O$ (−19.02–−4.39‰) of freshwater carbonates [51], respectively, and the $^{87}Sr/^{86}Sr$ ratios are significantly higher than those of the Neogene seawater, which are plotted between the ratios of the modern river and the Earth's crust (Figure 5), indicating that the mudstones are deposited in continental freshwater.

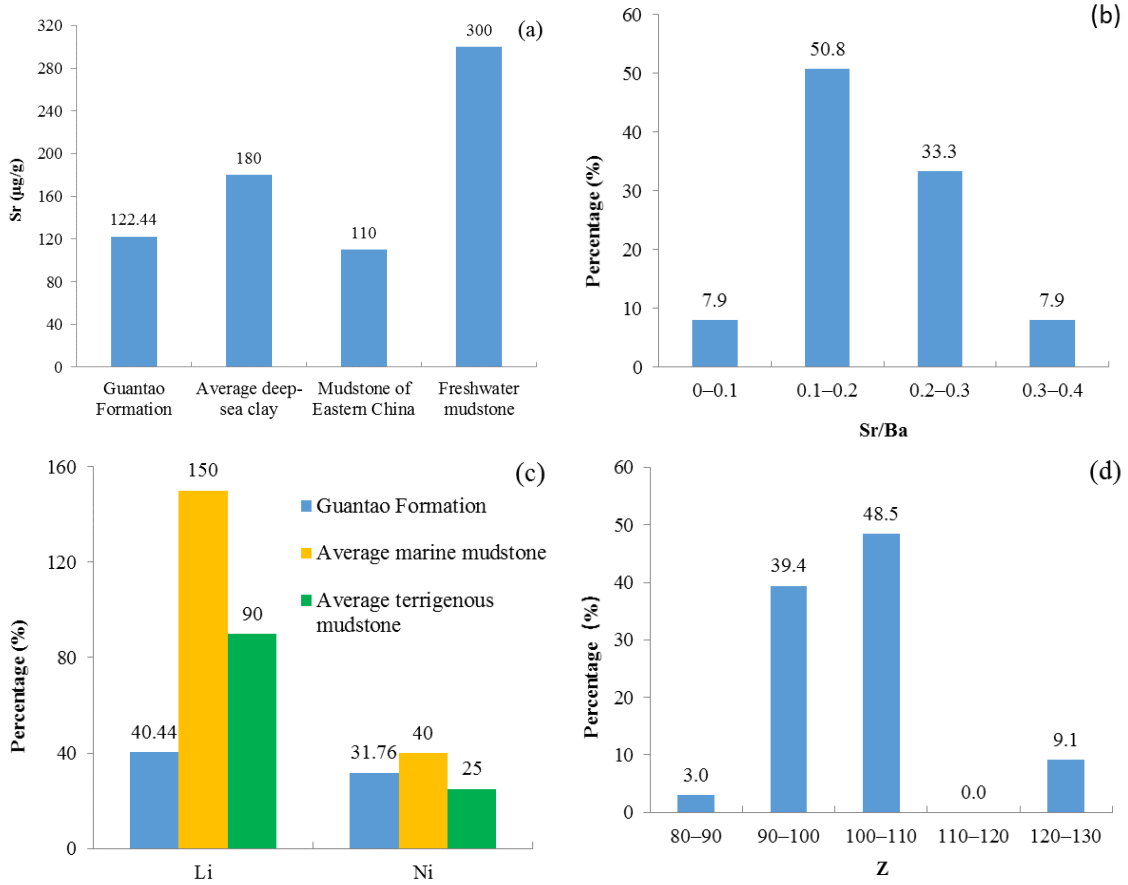

Figure 6. (**a**) Comparison diagram of Sr content of the Guantao Formation with average marine mudstone [43], mudstone of Eastern China and freshwater sediments [58]. (**b**) Distribution histogram of Sr/Ba ratios. (**c**) Comparison diagram of Li and Ni content of the Guantao Formation with the average marine mudstone [43] and the average terrigenous mudstone [58]. (**d**) Z value distribution histograms of the Guantao Formation.

Sedimentary paleosalinity can be roughly identified using the salinity indication index Z calculated by the empirical equation (1) established by Keith and Weber (1964) [51]. With the exception of three samples with Z greater than 120, the Z of all samples is less than 120 (Figure 6d), indicating that the sedimentary environment of the Guantao Formation is mainly freshwater.

$$Z = 2.048 \times (\delta^{13}C + 50) + 0.498 \times (\delta^{18}O + 50) \quad (1)$$

Above all, the Guantao Formation mainly consists of continental freshwater deposits.

5.4.2. Paleotemperature

The sedimentary paleotemperature range of the Guantao Formation is 28.82–31.27 °C (mean 30.39 °C), calculated by the empirical Equation (2) [59], which is established based on the relationship between the sedimentary temperature (T_{Sr}, °C) and Sr content (y, μg/g).

$$T_{Sr} = (2578 - y)/80.8 \quad (2)$$

$\delta^{18}O_{SMOW} = -5‰$ of the present meteoric water from the coast of China is selected as the $\delta^{18}O$ value of the sedimentary water in the study area because the Guantao Formation is mainly deposited from continental freshwater, and the paleosedimentary temperature (T_O, °C) is calculated by the calcite–water fractionation equation (0–500 °C) (3) proposed by Friedman and O'Neil (1977) [60]. The oxygen isotope temperatures of the Guantao

Formation range from 11.0 °C to 57.5 °C, with an average of 29.8 °C, and the temperatures in 66.7% of the samples range from 20 °C to 50 °C (Figure 7), which is roughly equivalent to the sedimentary temperatures calculated according to the Sr content. Moreover, 6.1% of the samples with temperatures exceeding 50 °C may be related to the burial heating process.

$$1000\ln\alpha_{\text{calcite-water}} = 2.78 \times 10^6 \times T_O^{-2} - 2.89 \quad (3)$$

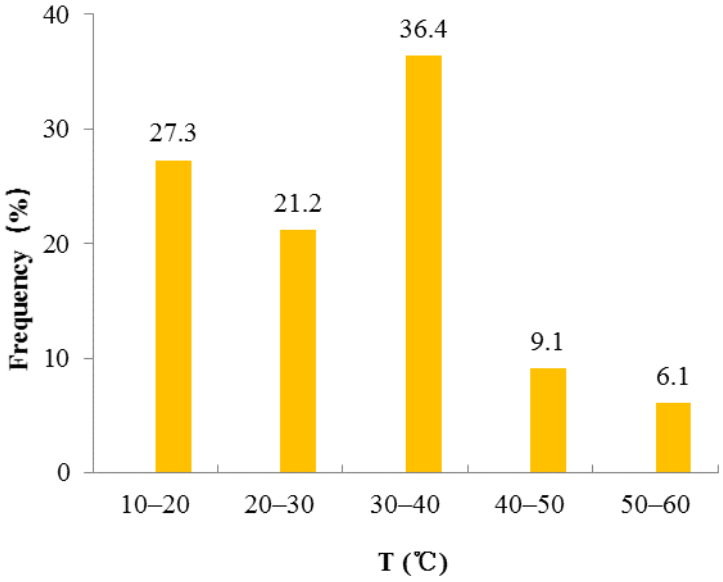

Figure 7. Distribution histogram of temperatures calculated by the calcite–water fractionation equation.

In Equation (3), $\alpha_{\text{calcite–water}}$ is the oxygen isotope fractionation coefficient between calcite and water.

Above all, the paleotemperatures of the Guantao Formation in the Liaodong sub-uplift indicate subtropical–tropical conditions, which is consistent with the research results indicating that the paleoclimate during the Guantao Formation's deposit was subtropical with the use of the semi-quantitative method of plant palynology [28].

5.4.3. Paleodepth

Mn has strong oxidation resistance and can migrate over a long distance, but the stability of Ti is relatively weak and it cannot migrate far [7,23]. Therefore, the Mn/Ti ratio is inversely proportional to the offshore distance. The average Mn/Ti ratios of alluvial plain, lacustrine delta front + shore shallow lake and semi-deep lake + prodelta could be summarized as 0.05, 0.15, and 0.30, respectively [22,61]. The Mn/Ti ratios of the Guantao Formation range from 0.01 to 1.22 (mean 0.08), and 87.7% of the values are far lower than 0.15. Therefore, the Guantao Formation is mainly formed in a nearshore shallow water environment.

The average abundance of Co as a typical element of cosmic dust is 4000 ug/g in cosmic dust, and the falling rate of cosmic dust on the Earth is relatively constant (approximately 1.6×10^{-4} g/cm^2.year), so the Co content in sediments is obviously controlled by the deposition rate. According to the above principle, Wu and Zhou (2000) [61] and Zhou et al. (1998) [62] proposed two Equations (4) and (5) for calculating the sedimentation rate and paleowater depth (h) by using the Co content.

$$V_s = V_o \times N_{Co}/(S_{Co} - t \times T_{Co}) \quad (4)$$

$$H = 3.05 \times 10^5/V_s^{1.5} \quad (5)$$

where V_s is the study sample sedimentation rate, and the upper limit deposition rate of 300 m/Ma of the normal lacustrine mudstone [7] is selected as the standard sedimentation rate V_o, because the Bohai Bay Basin experienced rapid subsidence in the Neogene, and the Co content of 20 ug/g [16] of the normal lacustrine sediments is selected as N_{Co}. Moreover, S_{Co} is the Co content of the study samples, t is the contribution of continental provenance to the Co of the study sample, which is the La ratio of the study sample and the average mudstone (La = 92 ug/g) [43], and T_{Co} is the background value of Co of the provenance at which the average Co content of 19 ug/g [43] of the average mudstone is selected.

According to the relationship between the palaeontologic growth characteristics and water depth of continental lakes, 0–15 m, 15–30 m, and >30 m can be used as division standards of shallow, semi-deep, and deep-water environments, respectively [24,63]. The calculated paleowater depth of the Guantao Formation is 0.04–60.16 m (average 10.14 m), and 68.8% and 14.1% belong to shallow and semi-deep environments, respectively (Figure 8). Moreover, the color of most of the mudstones of the Guantao Formation is gray–green and gray–white, which indicate underwater weak reduction conditions under the shallow environment [64]. Consequently, it could be concluded that the Guantao Formation is mainly the product of semi-deep and shallow water, which is essentially consistent with the results of the paleowater depth of 0–20 m of the Guantao Formation in the adjacent regions, inferred from paleontology by Mi et al. (2004) [65] and Pan et al. (2019) [33].

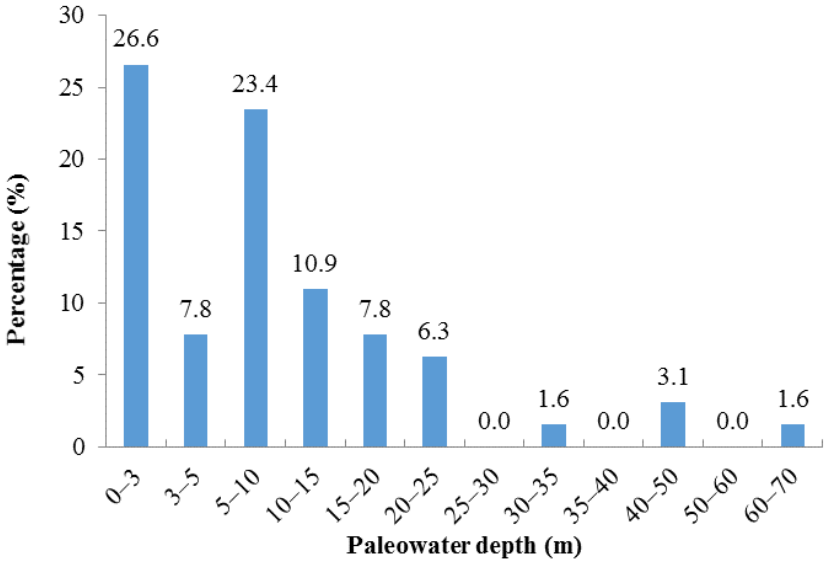

Figure 8. Distribution histogram of paleodepths of the Guantao formation in the Liaodong sub-uplift.

5.4.4. Redox State

The enrichment degree of trace elements such as U, V, Cr, Ni, and Co is controlled by the redox conditions [66], and the most reliable redox discriminant indexes include the U/Th, V/Cr, and Ni/Co ratios [17]. U/Th, V/Cr, and Ni/Co greater than 1.25, 4.25, and 7 indicate reduction conditions, respectively; values less than 0.75, 2, and 5 indicate oxidation conditions, respectively; and values between the above ratios indicate dysoxic conditions, respectively. Here, 100% of U/Th, 100% of V/Cr, and 95.4% of Ni/Co values for the Guantao Formation are less than 0.75, 2, and 5 (Table 2), indicating an oxidizing state, which is strongly related to the shallow water environment.

5.5. Sedimentary Environment Characteristics

Liu and Liu (2017) [67], Pan et al. (2019) [33], and Yang et al. (2016) [63] studied the Mesozoic and Cenozoic lacustrine facies of Western and Eastern China, and considered that fluvial, lacustrine delta (or shore shallow lake), semi-deep-lake, and deep-lake environments correspond to the water depths of 0–3 m, 3–15 m, 15–30 m, and >30 m, respectively.

According to the paleodepth calculated by Equation (5), the Guantao Formation is mainly dominated by lacustrine delta (or shore shallow lake) facies, followed by semi-deep lake and fluvial facies, and rarely includes semi-deep and deep lake facies.

According to the general understanding that the total content ($T_{V+Ni+Cu}$) of V, Ni, and Cu gradually increases from fluvial to lacustrine facies in continental mudstones, Liu et al. (1986) established a standard of $T_{V+Ni+Cu}$ for dividing the sedimentary facies of the Cretaceous mudstones in the Songliao Basin of Heilongjiang Province, China (Deng and Qian, 1993 [23]), and the indicator has been effectively applied in other sedimentary basins in China, such as the Laiyang Basin in Shandong Province [32] and the Jianghan Basin in Hubei Province [67]. The trace elements of the modern fluvial and lacustrine sediments [68,69] are used to adjust the above standard to improve its accuracy, and the following standards for distinguishing continental sedimentary facies by $T_{V+Ni+Cu}$ are established: the $T_{V+Ni+Cu}$ of fluvial, shore-shallow-lake, semi-deep-lake, and deep-lake facies are <130 ug/g, 130–170 ug/g, 170–190 ug/g, and >190 ug/g, respectively. The $T_{V+Ni+Cu}$ of the Guantao Formation in the Liaodong sub-uplift varied from 78.15 ug/g to 196.27 ug/g (mean 142.54 ug/g), and 29.2% and 56.9% of the samples were located in the fluvial and shore shallow lake facies (Figure 9), indicating that the Guantao Formation was mainly deposited in the shore shallow lake, followed by the fluvial and semi-deep lake environment.

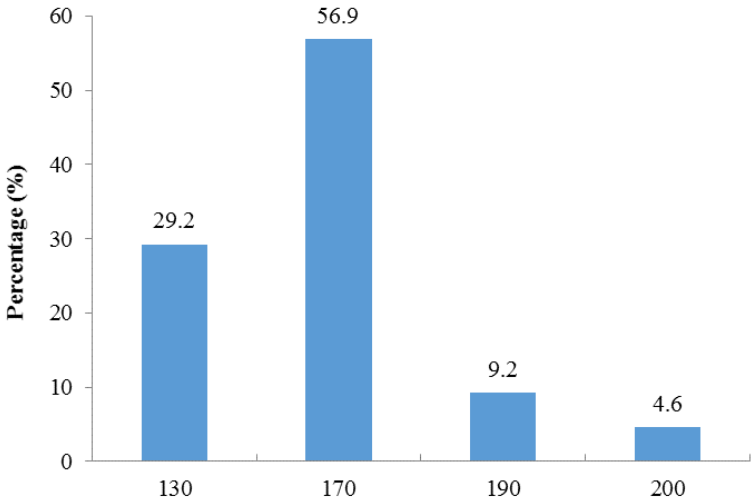

Figure 9. Distribution histogram of $T_{V+Ni+Cu}$ of the Guantao Formation in the Liaodong sub-uplift.

All $\delta^{13}C$ and $\delta^{18}O$ values of the Neogene Guantao Formation are plotted in the third quadrant (Figure 10) of the lacustrine sedimentary type analysis chart, and they overlap with the typical open lake and humid climate zones, which indicates that the Guantao Formation mainly originates from freshwater, and the climate during its sedimentation period was warm and humid; the negative $\delta^{13}C$ values are mainly related to organisms.

Based on the above analysis results, and combined with the research results of other scholars on the sedimentary facies of the Bohai Bay Basin, it can be judged that the sedimentary environment of the Guantao Formation in the Liaodong sub-uplift mainly consists of a shore shallow lake and braided river delta, followed by the fluvial and semi-deep lake. According to the color, lithology combinations, and logging facies, the Guantao Formation of well JZ17 is mainly deposited in braided-river delta-front subfacies (Figure 11), which is consistent with the above analysis results of the sedimentary environment, indicating that geochemical methods have high accuracy in identifying the sedimentary environment.

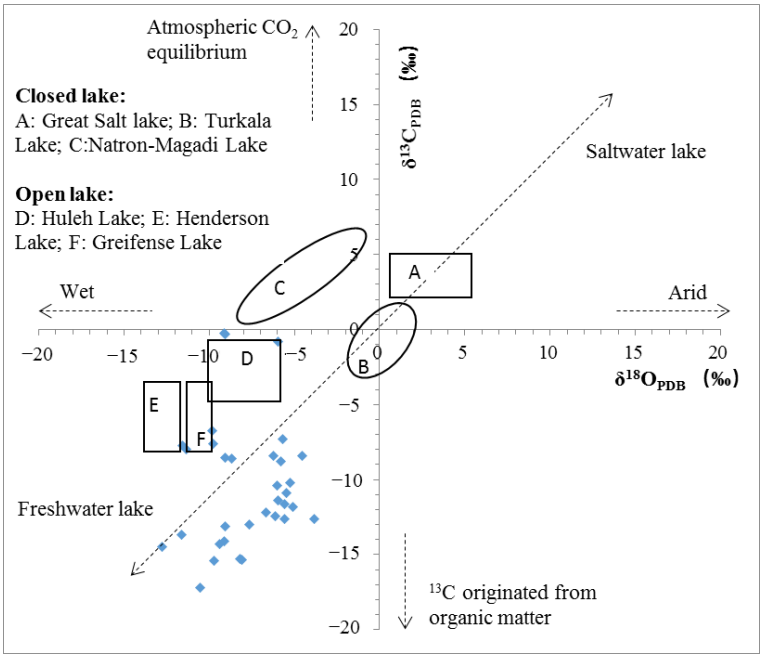

Figure 10. Lacustrine sedimentary type analysis chart [47] based on carbon and oxygen isotope values.

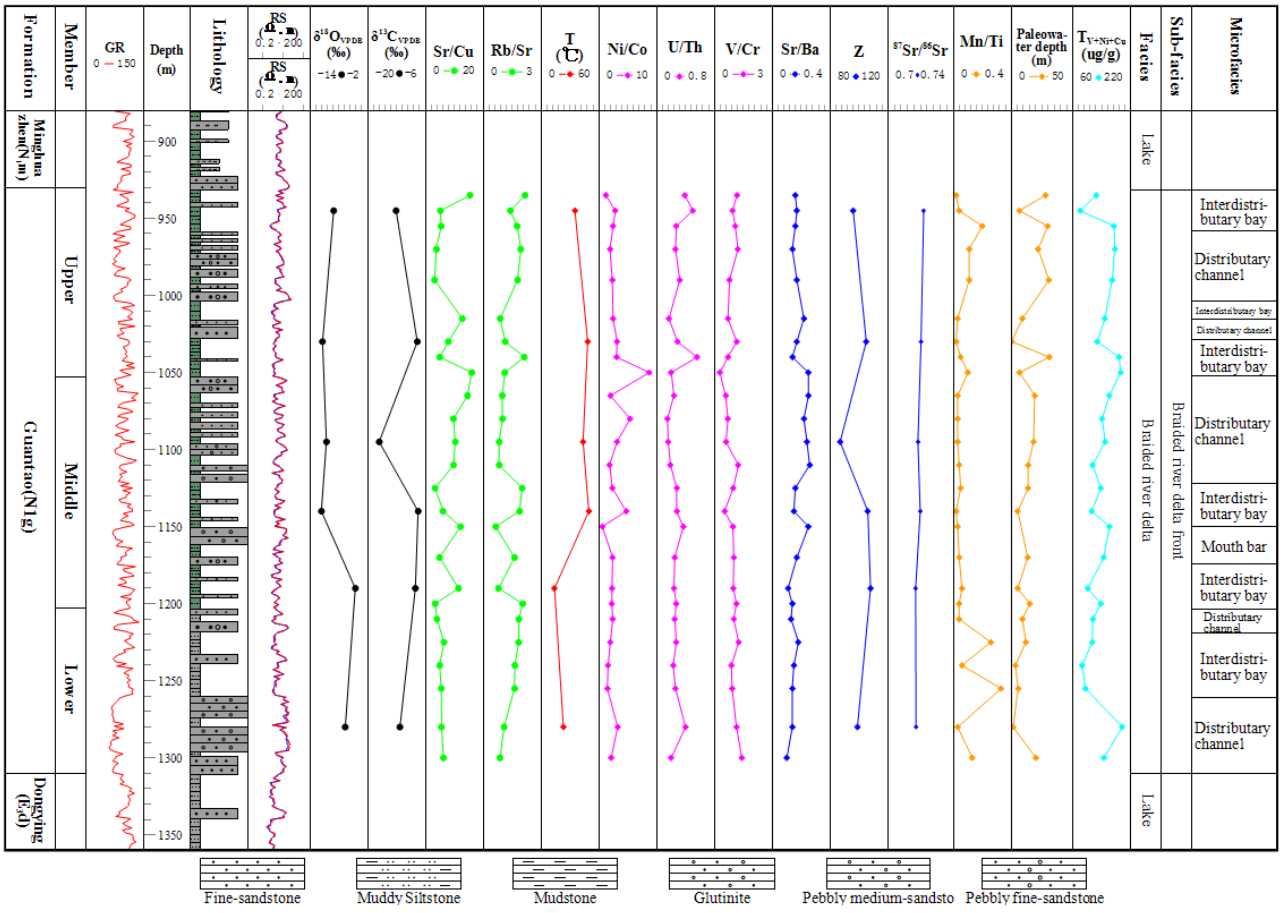

Figure 11. Temporal variations in geochemistry parameters representing paleoenvironment and paleoclimate evolution of the Guantao Formation (Well JZ17).

5.6. Evolution of Sedimentary Environment and Paleoclimate

Well JZ17 (Figure 11), with relatively complete trace element and isotope data, is selected to analyze the sedimentary environment and paleoclimate evolution, which could be a good regional representative.

In the early sedimentary stage (corresponding to the Lower Member) of the Guantao Formation, the paleotemperature and Sr/Cu decreased but Rb/Sr increased, showing that the climate gradually became wet and cold. The paleowater depth and $T_{V+Ni+Cu}$ gradually increased, and Sr/Ba increased firstly and then decreased, showing that the water body was gradually desalinated and became deeper. Ni/Co, V/Cr, and U/Th fluctuated only slightly, indicating the oxidation state.

In the middle stage (corresponding to the Middle Member), $\delta^{13}C$ reached the maximum, $\delta^{18}O$ decreased, and the paleotemperature, Sr/Cu, Sr/Ba, Z index, paleowater depth, and $T_{V+Ni+Cu}$ gradually increased to the maximum, indicating that the climate gradually became hot and humid, and the water body gradually became salty and deeper. V/Cr and U/Th changed less compared with the values in the early stage, but Ni/Co increased significantly, indicating that the reducibility of the sedimentary environment increased due to the increase in water depth in the middle stage.

In the late stage (corresponding to the Upper Member), $\delta^{18}O$ increased, and the paleotemperature, $\delta^{13}C$, Sr, Sr/Cu, Sr/Ba, and Z index gradually decreased, while the paleodepth and $T_{V+Ni+Cu}$ gradually increased to the maximum, which reflect the warm and humid climate and relatively deeper and fresher water. Additionally, Ni/Co, V/Cr, and U/Th were equivalent to those in the early and middle stages, which indicates oxidizing conditions. On the whole, from early to late, the sedimentary environment of the Guantao Formation was characterized by an increasing temperature, humidity, and water depth, and decreasing salinity and oxidizing state. Furthermore, $^{87}Sr/^{86}Sr$ and Rb/Sr increased gradually, indicating that the chemical weathering was gradually enhanced.

Generally, from early to late, the temperature and humidity gradually increased; the chemical weathering effect and the water depth gradually increased and the salinity gradually decreased due to increasing precipitation.

6. Conclusions

(1) The trace element distribution patterns resemble that of the intermediate–acidic magmatic rock in East China; clay minerals mainly consist of I/S mixed-layer clay minerals and illites, and continental elements Ti, Zr, and Th are highly concentrated, which indicates that the provenance of the Guantao Formation in the Liaodong sub-uplift mainly originates from the intermediate–acidic magmatic rocks near surrounding uplifts.

(2) Sr/Cu ratios mainly in the range of 5–10 reveal semi-arid and semi-humid conditions, and the high Rb/Sr and $^{87}Sr/^{86}Sr$ ratios further confirm that the climate of the Guantao Formation in the Liaodong sub-uplift is relatively warm and humid.

(3) Li, Ni, and Sr content, Sr/Ba ratios, $^{87}Sr/^{86}Sr$ ratios, and salinity index Z are in the continental freshwater zone in most mudstones, which shows that the Guantao Formation in the Liaodong sub-uplift was deposited in continental freshwater.

(4) The paleosedimentary temperature calculated by the Sr content and $\delta^{18}O$ was roughly equivalent, both with an average of around 30 °C, indicating that the Guantao Formation in the Liaodong sub-uplift was deposited in a subtropical to tropical climate.

(5) Most Mn/Ti ratios were less than 0.15, and the vast majority of the paleowater depths calculated based on the Co content were less than 30 m, which reflects that the Guantao Formation in the Liaodong sub-uplift was mainly deposited in nearshore shallow water.

(6) Most of the U/Th, V/Cr, and Ni/Co ratios were less than 0.75, 2, and 5, indicating that the Guantao Formation in the Liaodong sub-uplift was deposited in an oxidizing condition, and it is in a good coupling relationship with the shallow sedimentary environment.

(7) The sedimentary environment of the Guantao Formation in the Liaodong sub-uplift mainly belongs to a shore shallow lake and braided river delta, followed by a fluvial environment and semi-deep lake.
(8) From early to late, the temperature, humidity, and water depth of the Guantao Formation in the Liaodong sub-uplift gradually increased, the salinity gradually decreased, and the chemical weathering effect gradually increased.

Author Contributions: Conceptualization, Z.L. (Zhengxiang Lv), S.N.; Formal analysis, Y.L.; Funding acquisition, M.W. and S.N.; Investigation, Z.L. (Zheyuan Liao); Methodology, Y.Q.; Project administration, Z.L. (Zhengxiang Lv) and S.N.; Resources, J.F., S.T. and Y.Y.; Software, S.L.; Supervision, Z.L. (Zhengxiang Lv).; Validation, Y.Q.; Visualization, Y.Q.; Writing—original draft, M.W. and Y.Q.; Writing—review and editing, Y.Q. All authors have read and agreed to the published version of the manuscript.

Funding: This study was supported by funds from CNOOC Energy Development Co., Ltd. (No. HFKJ-GJ2016004).

Institutional Review Board Statement: Not applicable.

Informed Consent Statement: Not applicable.

Data Availability Statement: Data sharing is not applicable to this article.

Acknowledgments: We thank the anonymous reviewers for their careful reviews and detailed comments. We also thank the CNOOC Energy Development Co., Ltd., Tianjin, China for data support.

Conflicts of Interest: The authors declare that there is no conflict of interest with respect to the research, authorship, and/or publication of this article.

References

1. Selley, R.C. *Applied Sedimentology*, 2nd ed.; Academic Press: San Diego, CA, USA, 2000.
2. Boggs, S., Jr. *Principles of Sedimentology and Stratigraphy*, 4th ed.; Pearson Education, Inc.: New York, NY, USA, 2006.
3. Demaison, G.J.; Moor, G.T. Anoxic environments and oil source bedgenesis. *J. AAPG Bull.* **1980**, *64*, 1179–1209.
4. Adepehin, E.J.; Bankole, O.M.; Arifin, M.H. Poro-perm evolution in Oligo-Miocene coastal sandstones: Constraining the relative influence of sedimentary facies, mineralogy, and diagenesis on analogue reservoir quality of the Nyalau Formation, Borneo. *Mar. Pet. Geol.* **2022**, *139*, 1–22. [CrossRef]
5. Curtis, C.D. Sedimentary geochemistry: Environments and processes dominated by involvement of an aqueous phase. Philosophical Transactions of the Royal Society of London. *Ser. A Math. Phys. Sci.* **1977**, *286*, 353–372.
6. Albarède, F. *Geochemistry: An Introduction*, 2nd ed.; Cambridge University Press: Cambridge, UK, 2009.
7. Tian, J.C.; Zhang, X. *Sedimentary Geochemistry*; Geological Publishing House: Beijing, China, 2016. (In Chinese)
8. Zhou, X.Q.; Chen, D.Z.; Liu, M.; Hu, J.F. The Future of Sedimentology in China: A Review and Perspective of Sedimentary Geochemistry. *Acta Sedimentol. Sin.* **2017**, *35*, 1293–1316.
9. Balaram, V. Current and emerging analytical techniques for geochemical and geochronological studies. *Geol. J.* **2021**, *56*, 2300–2359. [CrossRef]
10. Subramanian, M.; Muthumanickam, J.; Karthikeyan, S.; Senapathi, V.; Viswanathan, P.M.; Sekar, S.; Sabarathinam, C. Elemental geochemistry of surface sediments from Manakudy estuary, south–west coast of India: Inferences to sources of elements and their accumulation. *J. Geol. J.* **2021**, *56*, 2360–2378. [CrossRef]
11. Algeo, T.J. Can marine anoxic events draw down the trace element inventory of seawater? *Geology* **2004**, *32*, 1057–1060. [CrossRef]
12. Cai, G.Q.; Guo, F.; Liu, X.T.; Sui, S.L. Carbon and oxygen isotope characteristics and palaeoenvironmental implications of lacustrine carbonate rocks from the Shahejie Formation in the Dongying Sag. *Earth Environ.* **2009**, *37*, 347–354, (In Chinese with English abstract).
13. Chang, H.J.; Chu, X.L.; Feng, L.J. Redox sensitive trace elements as paleoenvironments proxies. *Geol. Rev.* **2009**, *55*, 91–99. (In Chinese with English abstract)
14. Tribovillard, N.; Algeo, T.J.; Lyons, T.; Riboulleau, A. Trace metals as paleoredox and paleoproductivity proxies: An update. *Chem. Geol.* **2006**, *232*, 12–32. [CrossRef]
15. Shi, J.; Huang, W.H.; Lv, C.H.; Cui, X.N. Geochemical characteristics and geological significance of the Upper Paleozoic mudstones from Linxing area in Ordos Basin. *Acta Pet. Sin.* **2018**, *39*, 876–889. (In Chinese with English abstract)
16. Wang, D.R.; Guan, P.; Zhou, Z.H. Calculation of tectonic uplift of eastern Qaidam basin in Quaternary: Depending on the oxygen isotopic compositions within mudstone. *Pet. Explor. Dev.* **1998**, *25*, 39–40. (In Chinese with English abstract)
17. Jones, B.; Manning, D.A.C. Comparison of geochemical indices used for the interpretation of palaeoredox conditions in ancient mudstones. *Chem. Geol.* **1994**, *111*, 111–129. [CrossRef]

18. Rimmer, S.M. Geochemical Paleoredox Indicators in Devonian–Mississippian Black Shales, Central Appalachian Basin (USA). *Chem. Geol.* **2004**, *206*, 373–391. [CrossRef]
19. Wang, W. Trace Elements as Redox Paleoenvironments Proxies in Xiamaling Formation of the Mesoproterozoic in North China and Their Geological Significances. Master's Thesis, China University of Geosciences, Beijing, China, 2014. (In Chinese with English abstract)
20. Peng, J.J.; Zhang, M.; Liu, G.X.; Pan, W.L. Sedimentary environments and controlling factors of Permian source rocks in northeastern Sichuan Basin: A case study of Muguakou profile in Chengkou. *Pet. Geol. Exp.* **2014**, *36*, 95–101.
21. El–Anwar, E.A.A.; Mekky, H.S.; Wahab, W.A. Geochemistry, mineralogy and depositional environment of black shales of the Duwi Formation, Qusseir area, Red Sea coast, Egypt. *Carbonates Evaporites* **2019**, *34*, 883–892. [CrossRef]
22. Liu, B.L. *Fundamentals of Geochemistry*; Peking University Press: Beijing, China, 1994. (In Chinese)
23. Deng, H.W.; Qian, K. *Sedimentary Geochemistry and Environmental Analysis*; Gansu Science and Technology Press: Lanzhou, China, 1993. (In Chinese)
24. Liang, Z.R.; Hou, M.C.; Cao, H.Y.; Chao, H. Elemental Geochemistry characteristics of Jurassic and indication of sedimentary environment of Shiguai Basin, Daqingshan, Inner Mongolia. *J. Chengdu Univ. Technol. (Sci. Technol. Ed.)* **2020**, *47*, 307–317. (In Chinese with English abstract)
25. Farrell, Ú.C.; Samawi, R.; Anjanappa, S.; Klykov, R.; Adeboye, O.O.; Agic, H.; Anne-Sofie, A.C.; Boag, T.H.; Bowyer, F.; Brocks, J.J.; et al. The Sedimentary Geochemistry and Paleoenvironments Project. *Geobiology* **2021**, *19*, 545–556. [CrossRef]
26. Chen, C. Study on the Coupling Dynamic Process of Hydrocarbon Accumulation of Liaodong Depression. Master's Thesis, Chengdu University of Technology, Chengdu, China, 2016. (In Chinese with English abstract)
27. Liu, T. Sedimentology and Provenance Analysis of Paleogene–Neogene Strata in the Eastern Bohai Bay Basin. Master's Thesis, China University of Geosciences, Beijing, China, 2020. (In Chinese with English abstract)
28. Zhong, Y.J.; Chen, H.D.; Xu, C.G.; Wang, J.; Zou, H.; Wei, P. Discovery of shallow–water delta in the Neogene Guantao Formation in the Liaodong Bay Depression and its significance for oil and gas exploration. *Oil Gas Geolog.* **2017**, *38*, 499–507. (In Chinese with English abstract)
29. Zhou, Y.; Li, H.L.; Zhang, R.; Liu, D.D. Characteristics of strike–slip faults in the northern part of Liaodong Salient and their control on hydrocarbon accumulation. *China Offshore Oil Gas* **2018**, *30*, 29–34. (In Chinese with English abstract)
30. Li, X.H.; Du, X.F.; Guan, D.Y.; Wang, Z.P.; Wang, Q.M. Sedimentary characteristics of braided–meandering transitional river of Neogene Guantao Formation in northeastern Liaodong Bay Depression. *Lithol. Reserv.* **2022**, *34*, 93–103.
31. Dai, L.M.; Li, J.P.; Zhou, X.H.; Cui, Z.G.; Cheng, J.C. Depositional system of the Neogene shallow water delta in Bohai Sea area. *Lithol. Reserv.* **2007**, *19*, 75–81. (In Chinese with English abstract)
32. Li, X.Q.; Gao, X.L.; Feng, C.; Bu, S.F.; Wang, G.Y. Depositional Environment of Guantao Formation in Western Bohai Sea and Its Petroleum Geology Significance. *J. Xi'an Shiyou Univ. (Nat. Sci. Ed.)* **2019**, *34*, 10–17.
33. Pan, W.J.; Liu, S.L.; Tian, D.R.; Guo, L.L.; Wang, X.L.; Wang, L.H. Reconstruction of palaeo–water depth of Neocene shrinking lake: An example from the south of Bodong Low Uplift, Bohai Sea. *Mar. Geol. Front.* **2019**, *35*, 18–25. (In Chinese with English abstract)
34. Liu, S.L.; Liu, Y.H.; Lin, G.; Zhou, Y.; Gong, F.X.; Zhang, D.S. REE Geochemical Characteristics and Geological Significance of Mudstones from Neogene, Nanpu Sag, Bohai Basin. *Geoscience* **2006**, *20*, 449–456. (In Chinese with English abstract)
35. Guo, J.X.; Gong, Y.W. Geochemical Characteristics and Geological Significance of Neogene System in Liuxi-Liubei Tectonic Zone in Raoyang Sag. *Geol. Sci. Technol. Inf.* **2018**, *37*, 41–49. (In Chinese with English abstract)
36. Xu, C.G.; Ren, J.; Wu, Z.P.; Li, W.; Zhang, J.; Zhang, X.Q. Cenozoic Fault System and Tectonic Evolution of the Eastern Liaodong Bay Depression. *Geol. J. China Univ.* **2015**, *21*, 215–222. (In Chinese with English abstract)
37. Zhang, H. Main Controlling Factors of Hydrocarbon Accumulation in Northeastern Liaodong Bay Depression. Master's Thesis, China University of Petroleum (East China), Qingdao, China, 2018.
38. Sun, Z.H.; Zhu, H.T.; Xu, C.G.; Du, X.F. Provenance Analysis of Neogene Guantao Formation in Bodong Sag, Bohai Bay Basin, Eastern China: Implications for Sediment Routing. In Proceedings of the AAPG Annual Convention and Exhibition, San Antonio, TX, USA, 19–22 May 2019.
39. Lin, G.S.; Xu, Z.B.; Wang, L.B.; Liu, Y.C.; Li, L.; Liang, S.H. Evolutions and their influences on the sedimentary system for Guantao Formation provenances in oilfield P of Bohai Bay Basin. *Pet. Geol. Oil Dev. Daqing* **2018**, *37*, 22–27. (In Chinese with English abstract)
40. Li, B.; Yang, H.X.; Liu, W. *Chemical Analysis Method for Clastic Rocks Part 30: Measurement of 44 Elements*; Standardization Administration of China: Beijing, China, 2010. (In Chinese)
41. Li, Z.S.; Li, X.C.; Ma, C.H. *Analytical Method for Carbon and Oxygen Isotopes in Organic Matter and Carbonate Rocks*; National Development and Reform Commission of China: Beijing, China, 2008. (In Chinese)
42. Zhang, G.C.; Cui, J.Y.; Gao, D.S. *Determinations for Isotopes of Lead, Strontium and Neodymium in Rock Samples*; Standardization Administration of China: Beijing, China, 1999. (In Chinese)
43. Turekian, K.K.; Wedepohl, K.H. Distribution of the elements in some major units of the earth's crust. *Geol. Soc. Am. Bull.* **1961**, *72*, 175–192. [CrossRef]
44. Yan, M.C. *Chemical Composition of Crust and Rocks in Eastern China*; China Science Publishing & Media Ltd.: Beijing, China, 1997. (In Chinese)

45. Guo, Y.Q.; Yu, F.; Li, Y.; Liang, D.Y.; Li, W.H.; Zhao, J.Z.; Ma, Y.P. Geochemical characteristics of sedimentary environment on He 8 Member of Shihezi Formation in eastern Ordos Basin. *Chin. J. Geol.* **2016**, *51*, 872–890. (In Chinese with English abstract)
46. Wu, Z.P.; Ma, Z.P.; Zhou, Y.Q. Element geochemical characters of sedimentary facies in the triassic–jurassic boundary section of Jiyuan Basin in Henan Province. *J. Univ. Pet. China* **2002**, *26*, 20–25.
47. Wang, Z.L. Study on the Origin of Loess like Material in Jinsha River Valley and Its Environmental Indicative Significance. Master's Thesis, Yunnan Normal University, Kunming, China, 2016. (In Chinese with English abstract).
48. Chen, L.; Shen, H.Y.; Jia, Y.L.; Wu, J.L.; Li, X.S.; Wei, L.; Wang, P.L. Environmental change inferred from Rb and Sr of lacustrine sediments in Huangqihai Lake, Inner Mongolia. *J. Geogr. Sci.* **2008**, *3*, 373–384. (In Chinese with English abstract) [CrossRef]
49. Liu, B.J. *Sedimentary Diagenesis*; China Science Publishing & Media Ltd.: Beijing, China, 1992. (In Chinese)
50. Irwin, H.; Curtis, C.; Coleman, M. Isotopic evidence for source of diagenetic carbonates formed during burial of organic–rich sediments. *Nature* **1977**, *269*, 209–213. [CrossRef]
51. Keith, M.L.; Weber, J.N. Carbon and oxygen isotopic composition of selected limestones and fossils. *Geochim. Cosmochim. Acta* **1964**, *28*, 1787–1816. [CrossRef]
52. Kuznetsov, A.B.; Semikhatov, M.A.; Gorokhov, I.M. Strontium isotope stratigraphy: Principles and state of the art. *Stratigr. Geol. Correl.* **2018**, *26*, 367–386. [CrossRef]
53. Oing, H.R.; Veizer, J. Oxygen and carbon isotopic composition of Ordovician brachiopods: Implications for coeval sea–water. *Geochim. Cosmochim. Acta* **1994**, *58*, 4429–4442.
54. Ying, F.X.; Luo, P.; He, D.B. *Diagenesis and Diagenesis Numerical Simulation of Clastic Reservoir in Petroliferous Basins of China*; Petroleum Industry Press: Beijing, China, 2004.
55. Guo, H.L.; Wang, D.R. Stable isotopic composition and origin analysis of the carbonate cements within sandstone reservoirs of Tarim oilgas bearing area. *Petrol. Explor. Dev.* **1999**, *3*, 31–32. (In Chinese with English abstract)
56. Zhao, X.Y.; He, D.B. *Clay Mineral and Application in Oil and Gas Exploration and Development*; Petroleum Industry Press: Beijing, China, 2016; pp. 13–45.
57. Chang, F.Q.; Zhang, H.C.; Lei, G.L.; Pu, Y.; Chen, G.J.; Zhang, W.X.; Yang, L.Q. Geochemical behaviors of strontium isotope and related elements of the lacustrine deposits and their application to paleoenvironment reconstruction: A case tudy from Shell Bar section of Qaidam Basin. *Quat. Res.* **2010**, *30*, 962–971. (In Chinese with English abstract)
58. Liu, G.; Zhou, D.S. Application of microelements analysis in identifying sedimentary environment: Taking Qianjiang Formation in the Jianghan Basin as an example. *Pet. Geol. Exp.* **2007**, *29*, 307–310. (In Chinese with English abstract)
59. Liu, J.H.; Wu, Z.X.; Yu, S.; Jia, D.H. Paleocence trace element geochemistry and its geological significance in Lishui Sag. *China Offshore Oil Gas* **2005**, *17*, 8–11. (In Chinese with English abstract)
60. Friedman, I.; O'Neil, J.R. *Compilation of Stable Isotope Fractionation Factors of Geochemical Interest*, 6th ed.; Michael Fleisher (Technical Editor); US Government Printing Office: Washington, DC, USA, 1977; Volume 440, pp. 1–12.
61. Wu, Z.P.; Zhou, Y.Q. Using the characteristic elements from meteoritic must in strata to calculate sedimentation rate. *Acta Sedimentol. Sin.* **2000**, *18*, 395–399. (In Chinese with English abstract)
62. Zhou, Y.Q.; Wu, Z.P.; Shi, B.Q. Applications of neutron activation analysis in sequence stratigraphy. *Earth Sci. Front.* **1998**, *5*, 143–149. (in Chinese with English abstract)
63. Yang, H.; Fu, Q.; Qi, Y.L.; Zhou, X.P.; Gong, N.; Huang, S.X. The Paleontology phase zones and its geological significance on the late Triassic Yanchang stage palaeo–lacustrine, *Ordos Basin*. *Acta Sedimentol. Sin.* **2016**, *34*, 688–693. (In Chinese with English abstract)
64. Ding, Y.; Zhang, C.M. Relationship between Sedimentary Rock Color and Diagenesis—Taking Baikouquan Formation in the Mahu Sag as an Example. In Proceedings of the National Sedimentology Conference, Wuhan, China, 16–22 October 2015.
65. Mi, L.J.; Bi, L.G.; Gong, S.L.; Wu, G.X.; Qin, J.G.; Shao, L.; Xia, P.F. Direct evidence for development of Bohai paleolake during the Neogene. *Mar. Geol. Quat. Geol.* **2004**, *24*, 37–42. (In Chinese with English abstract)
66. Tong, W.H. Geochemical Characteristics and Sedimentary Environment of Ore–Bearing Strata of Heqing Bauxite Deposit, Yunnan. Master's Thesis, Kunming University of Technology, Kunming, China, 2016. (In Chinese with English abstract)
67. Liu, Y.L.; Liu, P. Quantitative controls in water environment to distribution of sediments in saline lacustrine basin: A case of Es41 in Bonan Sag. *J. Cent. South Univ. (Sci. Technol.)* **2017**, *48*, 239–246. (In Chinese with English abstract)
68. Wang, C.L.; Liu, C.L.; Hu, H.B.; Mao, J.S.; Shen, L.J.; Zhao, H.T. Sedimentary characteristics and its environmental significance of salt–bearing strata of the Member 4 of Paleocene Shashi Formation in southern margin of Jiangling Depression, Jianghan Basin. *J. Palaeogeogr.* **2012**, *14*, 165–175.
69. Yang, S.Y.; Li, C.X.; Jung, H.S.; Lim, D.I.; Choi, M.S. Geochemistry of trace elements in Chinese and Korean river sediments. *Mar. Geol. Quat. Geol.* **2003**, *23*, 19–24. (In Chinese with English abstract)